JBC RESEARCH ARTICLE

FNDC5/irisin facilitates muscle–adipose–bone connectivity through ubiquitination-dependent activation of runt-related transcriptional factors RUNX1/2

Received for publication, August 27, 2021, and in revised form, January 25, 2022 Published, Papers in Press, February 4, 2022,
https://doi.org/10.1016/j.jbc.2022.101679

Xinyu He[‡], Yue Hua[‡], Qian Li, Wei Zhu, Yu Pan, Yilin Yang, Xinyang Li, Mengxiao Wu, Jiyong Wang[*], and Xiaoqing Gan[*]

From the Key Laboratory of Metabolism and Molecular Medicine, Ministry of Education, Department of Biochemistry and Molecular Biology, School of Basic Medical Sciences, Fudan University, Shanghai, China

Edited by George DeMartino

In the past decade, the cleavage protein irisin derived from fibronectin type III domain–containing protein 5 (FNDC5) in exercise-stimulated skeletal muscle has increasingly become a biomarker associated with metabolic syndrome and osteoporosis in humans. However, it is unclear how this protein facilitates muscle–adipose–bone connectivity in metabolic and skeletal homeostasis. In this study, we unexpectedly observed that the *FNDC5* gene can be markedly activated during the differentiation of brown adipocytes but not white adipocytes, and that FNDC5 is specifically expressed in mouse brown adipose tissues (BATs). But unlike it in the skeletal muscles, the expression of FNDC5/irisin in BAT is promoted by cold exposure rather than exercise in mice. Analysis of promoter activity and chromatin immunoprecipitation further showed that peroxisome proliferator–activated receptor γ coactivator-1α and thyroid hormone receptors cooperate on the *FNDC5* gene promoter to induce its transcription. We found that FNDC5/irisin stimulates the runt-related transcriptional factors RUNX1/2 *via* a focal adhesion kinase–dependent pathway in both bone and subcutaneous white adipose tissues. Mechanistically, focal adhesion kinase is stimulated by FNDC5/irisin and then facilitates E3 ubiquitin–protein ligase WW domain–containing protein 2 to ubiquitinate and subsequently activate RUNX1/2, culminating in the activation of osteoblast-related or thermogenesis-related genes. Interestingly, the PR domain containing protein 16 that is crucial for subcutaneous white adipose "browning" and skeletal development was found to form a complex with RUNX1/2 in a WW domain–containing protein 2-dependent manner. These findings elucidate a signaling mechanism by which FNDC5/irisin supports the muscle–adipose–bone connectivity, especially BAT–bone connectivity.

Adipose develops to obesity when energy intake far exceeds consumption, thereafter resulting in various metabolic disorders, such as hyperlipidemia, type 2 diabetes, and osteoporosis. There are two categories of adipose tissues in rodents and humans: the white adipose tissue (WAT) and the brown adipose tissue (BAT). The WAT deposits excessive energy as triglyceride, whereas the BAT promotes energy expenditure by incorporating the uncoupling protein 1 (UCP1) in the mitochondrial membranes, leading to burning of energy into CO_2 and water instead of ATP production (1–3). The WAT can also adopt the brown fat–like energy metabolism when undergoing a "browning" transdifferentiation (4). A growing body of evidence indicates that the adipose tissue is one of central metabolic organs highly integrated in energy homeostasis controlled by diverse interorgan communications. It not only produces multiple adipokines to affect energy metabolism but also is the main target of a wide variety of metabolic hormones, such as β3-adrenaline, fibroblast growth factor 21, as well as bone-derived osteocalcin (OCN; also known as bone gamma-carboxyglutamic acid–containing protein) (5–7).

In the past decade, a peroxisome proliferator–activated receptor γ coactivator-1α (PGC1α)–dependent myokine irisin has become relevant in metabolic homeostasis, as it facilitates "browning" of subcutaneous WAT (8). Irisin was first identified in the skeletal muscle of mice undergoing free-wheel exercise, as produced by the cleavage of the extracellular domain of the membrane protein fibronectin type III domain–containing protein 5 (FNDC5) (8). The administration of irisin in a range of 20 to 200 ng/ml can dramatically activate the expression of UCP1 in subcutaneous WATs (8). The mice mutant for FNDC5 has normal skeletal muscle development, body weight, and basal energy metabolism but exhibit damaged "browning" of subcutaneous WAT during exercise (9). Another report pointed out that lack of irisin leads to hyperlipidemia, insulin resistance, and poor energy metabolism (10). Furthermore, the altered expression of FNDC5 is associated with metabolic status in human being (11, 12), and FNDC5 single nucleotide polymorphisms are becoming an important diagnostic biomarkers for subjects with obesity and metabolic syndrome (13–15). Collectively, the correlation between the circulating irisin concentration and obesity/metabolic syndrome is increasingly becoming an area of research interest in prevention and prediction of metabolic disorders.

[‡] These authors contributed equally to this work.
[*] For correspondence: Xiaoqing Gan, xiaoqinggan@fudan.edu.cn; Jiyong Wang, jiyongwang@fudan.edu.cn.

Apart from adipose energy metabolism, lack of irisin is associated with reduced bone strength and bone mass in mice (10). Colaianni *et al.* (16) demonstrated that administration of recombinant irisin in healthy mice increases cortical bone mass and further hypothesized that the bone may be the primary target organ, as the dose of irisin in facilitating bone formation is much lower than that in "browning" of subcutaneous adipose tissues. The treatment of recombinant irisin can partially prevent the development of disuse-induced osteoporosis in "hind-limb suspended" mice (17). In postmenopausal women, circulating irisin concentration is negatively associated with vertebral fragility fractures (18, 19). Circulating irisin concentration may be a stronger determinant of bone mineral status than bone alkaline phosphatase in healthy children (20) and is positively associated with bone quality in children with type 1 diabetes mellitus (21). Hence, circulating irisin concentration is becoming one of the bone formation markers. In addition, FNDC5 expression and circulating irisin concentration have been shown to be associated with the inflammation, hippocampal neurogenesis, aging, and so on (22, 23). Taken together, irisin manifests as a multifunctional hormone to facilitate complex interorgan communication networks, thereby establishing the muscle–adipose–bone connectivity in metabolic and skeletal homeostasis.

Mitogen-activated protein kinase signaling pathways are thought to mediate the regulation of irisin in neural differentiation, white adipocyte "browning," as well as osteoblast differentiation (24–26). FNDC5 deficiency caused severe hepatosteatosis, upregulation of adenosine monophosphate–activated protein kinase, and downregulation of the mammalian target of rapamycin (27). Recently, irisin has been revealed to be capable of engaging integrin to facilitate the activation of focal adhesion kinase (FAK) in "browning" of white adipocytes (28). Nevertheless, the signaling mechanism employed by FNDC5/irisin to mediate the muscle–adipose–bone connectivity is still vague. One of open questions is how FNDC5/irisin signaling achieves gene transcription in the nucleus.

In the present study, we observed that cold exposure significantly stimulates the expression of *FNDC5* gene in the BAT and revealed that the cooperation of PGC1α and the thyroid hormone receptors (THRs) may contribute to *FNDC5* gene expression in cold-activated BAT. Unexpectedly, we evidenced that FNDC5/irisin stimulates the transcriptional activity of the runt-related transcriptional factors 1/2 (RUNX1/2) in osteoblasts and subcutaneous WAT *via* a FAK-dependent signaling pathway. Mechanistically, FNDC5/irisin signaling may activate FAK, which subsequently phosphorylates and activates E3 ubiquitin–protein ligase WW domain–containing protein 2 (WWP2). As a consequence, the transcriptional activity of RUNX1/2 is activated by WWP2-catalyzed ubiquitination. RUNX2 is a master transcriptional factor to facilitate expression of osteoblast genes including OCN. Interestingly, RUNX2 as well as its analog RUNX1 is preferentially expressed in the subcutaneous WAT compared with the visceral WAT and scapular BAT, accompanied by the dominant expression of the target gene *Ocn* in the subcutaneous WAT. In particular, perturbation of RUNX1/2 activities in the subcutaneous WAT not only inhibits the expression of *Ocn* but also damages the expression of UCP1 and "browning" of subcutaneous WAT. Consistent with these observations, the RUNX proteins can be complex with PR domain–containing protein 16 (PRDM16), which is crucial for the activation of *UCP1* gene promoter, and bind to the enhancer region upstream of the *UCP1* gene promoter. Taken together, the findings indicate that FNDC5/irisin is a cold-response factor in BAT, and we further evidence that FNDC5/irisin-facilitated muscle–adipose–bone connectivity may be mediated by the RUNX1/2 in the nucleus.

Results

Cold stimulates FNDC5/irisin expression in BATs

The *FNDC5* gene has been demonstrated to be activated in the skeletal muscle during exercises (8). Herein, we showed that it can also be activated during the adipogenic differentiation of adipose-derived stem cells (ADSCs) isolated from scapular BAT instead of subcutaneous WATs (Fig. 1, *A* and *B*). Consistently, the mRNA level of *Fndc5* gene in BAT is similarly higher than that in subcutaneous or gonadal WATs (Fig. 1*C*). Unlike it in the skeletal muscle, the *Fndc5* gene in BAT could not be activated by exercise (Fig. 1*C*). However, expression of FNDC5 expression in BAT can be significantly elevated by a long-term cold exposure lasting at least 1 day (Fig. 1*D*) or by a 10-day intermittent cold stimulation procedure (Fig. 1*E*). Therefore, *FNDC5* is also a cold-response gene of BAT, and even maintaining a short-time cold exposure daily can be of benefit to its expression. Although exercise does not directly activate the *Fndc5* gene of BATs (Fig. 1*C*), it can enhance cold induction of *Fndc5* gene expression in the BAT (Fig. 1*F*), indicating that the contraction of the skeletal muscle may indirectly affect BAT. In contrast to the BAT, the skeletal muscle facilitates *Fndc5* gene expression independently of ambient temperature (Fig. 1*F*). In addition, the expressions of *Fndc5* gene in heart, liver, and brain are also not affected by cold stimulation (Fig. 1*G*). Taken together, the results support a unique activation of *FNDC5* gene in the BAT upon cold exposure. Notably, the expression of FNDC5 in BAT can be significantly damaged by obesity, type 2 diabetes, as well as aging (Fig. 1, *H* and *I*). But unlike obese and diabetic mice, BAT of aging mice can still respond to cold stimulation (Fig. 1*I*).

Next, we explored the potential role of FNDC5/irisin in BAT function. We confirmed that knockdown of *FNDC5* gene expression in ADSCs derived from BAT could not affect the differentiation of brown adipocytes as well as the expression of thermogenesis genes in differentiated brown adipocytes (data not shown). In addition to energy metabolism, the cold-activated BAT augments bone mass, yet the mechanism is not fully understood (29–31). Our findings raise a possibility that the cold-activated BAT regulates bone remodeling through an FNDC5/irisin-mediated paracrine mechanism. Circulating irisin concentration has been reported to be positively associated with the mRNA level of *Ocn* gene

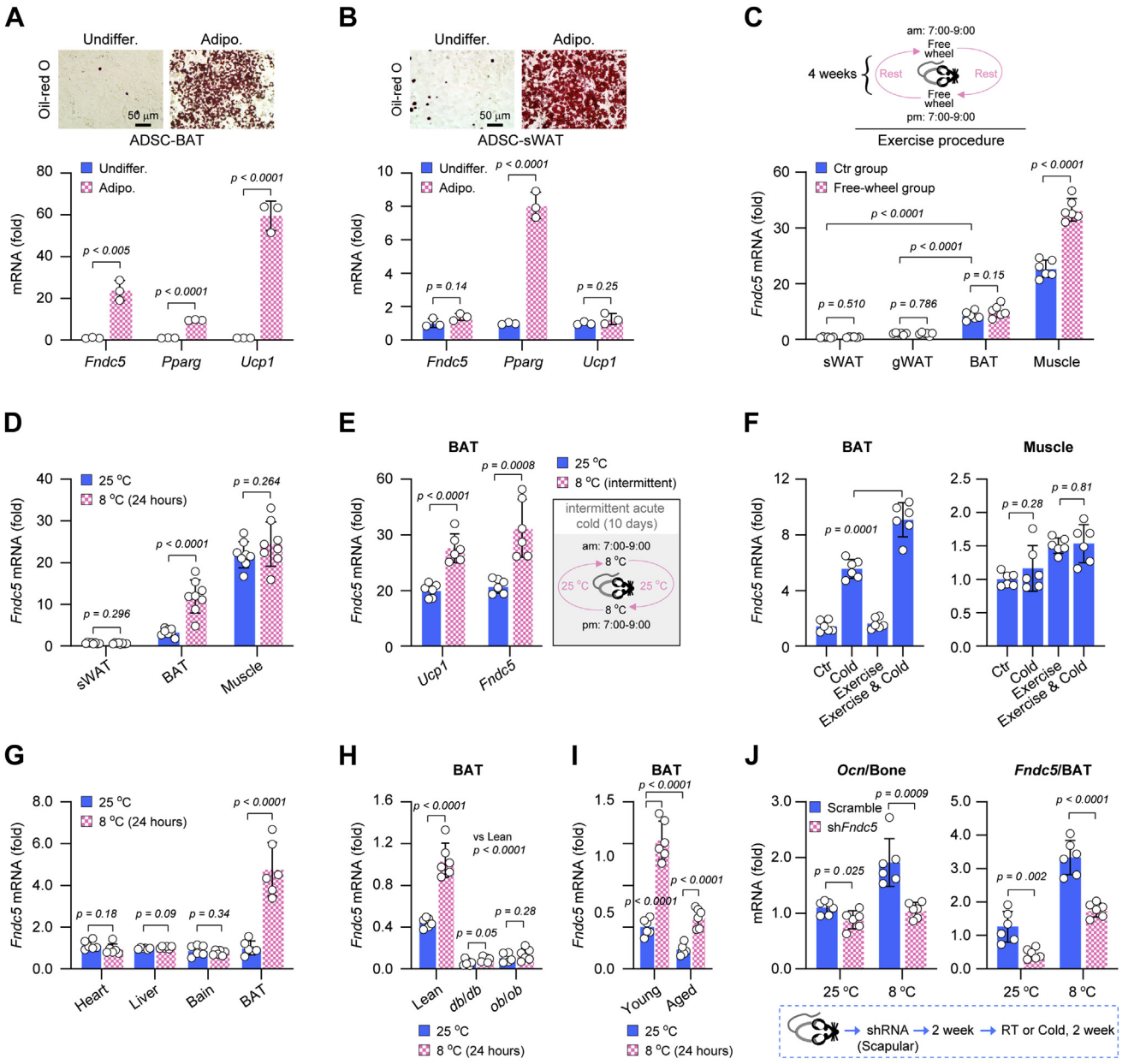

Figure 1. Cold stimulates FNDC5/irisin expression in brown adipose tissues (BATs). *A*, ADSCs derived from BAT were differentiated into brown adipocytes. Oil-Red O staining and mRNA examination were carried out at day 6 after differentiation (n = 3 biological replicates). *B*, ADSCs derived from subcutaneous WAT were differentiated into white adipocytes. Oil-Red O staining and mRNA examination were carried out at day 6 after differentiation (n = 3 biological replicates). *C*, *Fndc5* mRNA levels were examined in gWAT, sWAT, BAT, and skeletal muscle of 6-week-old mice. Mice were divided into two groups (n = 6 mice), the sedentary group as controls and the free-wheel group, which were subjected into 4-week free wheel exercise as described in the inserted schematic diagram. *D*, *Fndc5* mRNA levels were examined in sWAT, BAT, and skeletal muscle of 6-week-old mice. Mice were housed at room temperature (n = 8 mice) or 8 °C (n = 8 mice) for 24 h. *E*, *Fndc5* and *Ucp1* mRNA levels were examined in BAT of 6-week-old mice. Mice were housed at room temperature (n = 6 mice) or subjected into 2 h of cold exposure (8 °C) twice a day with an interval of 10 h as described in the inserted schematic diagram (n = 6 mice). After 10 days, mRNAs were extracted and examined. *F*, *Fndc5* mRNA levels were examined in BAT and skeletal muscle of 6-week-old mice. Mice were divided into four groups (n = 6 mice), the sedentary group at temperature as controls, the cold groups were housed in cool ambient (8 °C) for 1 week, the exercise group were housed in room temperature and underwent free-wheel running as indicated in (*C*) for 1 week, and the cold and exercise group were housed in cool ambient (8 °C) and underwent free-wheel running for 1 week as described for (*C*). *G*, *Fndc5* mRNA levels were examined in heart, liver, brain, and BAT of 6-week-old mice. Mice were housed at room temperature (n = 6 mice) or 8 °C (n = 6 mice) for 24 h. *H*, *Fndc5* mRNA levels were examined in BAT from lean mice (15 weeks old), diabetes mice (*db/db*, 14 weeks old), and obesity mice (*ob/ob*, 14 weeks old). Mice were housed at room temperature (n = 6 mice) or 8 °C (n = 6 mice) for 24 h, respectively. *I*, *Fndc5* mRNA levels were examined in BAT from young mice (8 weeks old) and aged mice (65–70 weeks old). Mice were housed at room temperature (n = 6 mice) or 8 °C (n = 6 mice) for 24 h, respectively. *J*, lentiviruses carrying scramble or *Fndc5* shRNA were injected into scapular BAT of 6-week-old mice as indicated, and then mice were housed at room temperature (n = 6 mice) or 8 °C (n = 6 mice) for 2 weeks. The mRNA levels of *Ocn* in tibia bone and *Fndc5* in BAT were measured. (All data are shown as the average values ± SD, two-tailed Student's *t* test was applied in *A* and *B*, and two-tailed ANOVA test was applied in *C*–*J*.). Adipo., adipogenesis; ADSC, adipose-derived stem cell; FNDC5, fibronectin type III domain–containing protein 5; gWAT, gonadal white adipose tissue; sWAT, subcutaneous white adipose tissue; Undiffer., undifferentiation; WAT, white adipose tissue.

encoding a noncollagen bone matrix protein (21, 32). When mice were housed in an ambient of 8 °C for 2 weeks, the expressions of *Ocn* gene in bone and *Fndc5* gene in BAT were both elevated (Fig. 1*J*). However, cold-induced expression of *Ocn* gene in bone was significantly attenuated by the knockdown of FNDC5 in the scapular BAT (Fig. 1*J*), where stores the main BATs of the mouse. Therefore, the results support the key physiological relevance of FNDC5/irisin in the paracrine function of BAT.

PGC1α and THR cooperate to facilitate FNDC5 *gene promoter*

Although the expression of FNDC5 is PGC1α dependent, PGC1α only moderately activates the *Fndc5* gene promoter, and meanwhile, the activation cannot be enhanced by peroxisome proliferator–activated receptor γ (PPARγ), unlike the activation of *Ucp1* gene promoter (Fig. 2*A*). In order to better understand the transcriptional machinery implicated in the activation of *FNDC5* gene promoter, we verified a series of master transcriptional factors expressed in the adipose and the skeletal muscle. In addition to PGC1α, the myogenic factors including MYF5, MYOD, and MYOG were identified to activate the *FNDC5* gene promoters (Fig. 2*B*). However, they cannot cooperate with PGC1α in the activation of *FNDC5* gene promoter (data not shown). The THRs are capable of activating PGC1α during adipocyte thermogenesis (33). Here, we observed that the coexpression of PGC1α and THRα dramatically activated *FNDC5* gene promoter (Fig. 2*C*), and the activation depends on an upstream promoter sequence away from the transcription initiation site (Fig. 2*D*). There are two putative THR-binding elements (thyroid hormone response element 1/2 [TRE1/2]) located in the region, and their deletion caused the activation of PGC1α and THRα to be weakened (Fig. 2*D*). We confirmed the interaction between PGC1α and THRα (Fig. 2*E*). Meanwhile, the deletion of TRE1/2 also significantly inhibits PGC1α-mediated promoter activation (Fig. 2*F*). Consistent with these findings, the chromatin immunoprecipitation (ChIP) experiments showed that TRE1/2 deletion impaired the occupation of THRα on the *ups3* promoter (Fig. 2*G*). At the same time, the re-ChIP experiment confirmed the colocalization of PGC1α with THRα on this region of *Fndc5* gene promoter (Fig. 2*G*). Therefore, these results indicate that PGC1α and THRα may rely on these TRE sites to form a transcriptional complex to manipulate *FNDC5* gene promoter.

Next, we investigated the regulation of the THR–PGC1α signaling on the activation *Fndc5* gene in BAT. Eight-week-old mice were fed with propylthiouracil (PTU) to block thyroxine synthesis *in vivo* or tetraiodothyronine (T4) to elevate plasma thyroxine levels. After 2 weeks, we observed that the scapular BAT was expanded, and the subcutaneous WAT was reduced in T4-diet mice (Fig. 2*H*). In contrast to T4 diet, PTU diet resulted in significant obesity of the subcutaneous WAT (Fig. 2*H*). More importantly, expression of *Fndc5* gene in the scapular BAT was significantly activated by T4 diet but suppressed by PTU diet (Fig. 2*H*). β3-adrenergic receptor (AR)-mediated signaling axis is involved in cold-activated BAT (34). Administration of β3-AR agonist CL316243 significantly stimulated *Fndc5* gene in scapular BAT, as compared with that in subcutaneous WAT (Fig. 2*I*). At the same time, treatment of compound H89, an inhibitor of cyclic AMP–dependent PKA downstream of the β3-AR signaling, resulted in significant reduction in the mRNA level of *Fndc5* gene in cold-activated BATs (Fig. 2*J*). Consistent with these examinations, constitutively active PKA catalytic subunit α dramatically enhances the cooperation of PGC1α and THRα on the *Fndc5* gene promoter (Fig. 2*K*). Taken together, these results demonstrate that cold exposure stimulates thyroxine and β3-AR–PKA signaling, ultimately leading to the cooperation of PGC1α and THR on *Fndc5* gene promoter in the BAT (Fig. 2*L*).

FNDC5/irisin stimulates the RUNX2 in osteoblasts

FNDC5/irisin has been profoundly implicated in bone formation (10, 16), but its signaling mechanism in this process is not yet fully elucidated. The hormone-like irisin (s-Irisin) that is fused with the signal peptide of interleukin 2 for secretory or nonsecretory irisin (ns-Irisin) that lacks the signal peptide was ectopically expressed in primary osteoblasts, which were then subjected into osteoblast differentiation (Fig. 3*A*). The ectopic expression of s-Irisin in osteoblasts could augment the mineral deposition during osteoblast differentiation compared with expression of GFP or ns-Irisin (Fig. 3*A*). As a master transcription factor of bone formation, the RUNX2 controls the expression of multiple osteoblast genes including *Ocn*, *Alpl* (*alkaline phosphatase*), *Osterix* (*sp7 transcription factor*), and so on. Notably, the ectopic expression of s-Irisin led to significant increase in expressions of these osteoblast genes but except for *Runx2* (Fig. 3*B*). At the same time, the transcriptional activity of RUNX2 on the *Ocn* gene promoter could be stimulated by s-Irisin rather than ns-Irisin (Fig. 3*C*). Taken together, the results indicate that RUNX2 may be regulated by FNDC5/irisin as an extracellular stimulus during osteoblast differentiation.

The recent study implicated FAK in the FNDC5/irisin signaling pathway (28). We observed that s-Irisin instead of ns-Irisin could induce FAK tyrosine phosphorylation in a FAK autophosphorylation-dependent manner (Fig. 3, *D* and *E*), indicating that FAK can be stimulated by the hormone-like irisin. Treatment of FAK inhibitor PF562271 could significantly impair the regulation of s-Irisin in osteoblast differentiation (Fig. 3*F*) as well as RUNX2 transactivation on the *Ocn* gene promoter (Fig. 3*G*). At the same time, ectopic expression of a constitutively active mutant of FAK (K38A) stimulates RUNX2 transcriptional activity (Fig. 3*H*). Therefore, the results support that the FNDC5/irisin signaling employs an FAK-dependent pathway to facilitate RUNX2 transactivation (Fig. 3*I*).

It is worth noting that s-Irisin did not induce FAK phosphorylation at Tyr-397 residue that is crucial for interaction with Src family kinase (Fig. 3*D*). At the same time, treatment of SRC inhibitor PP2 or ectopic expression of constitutively

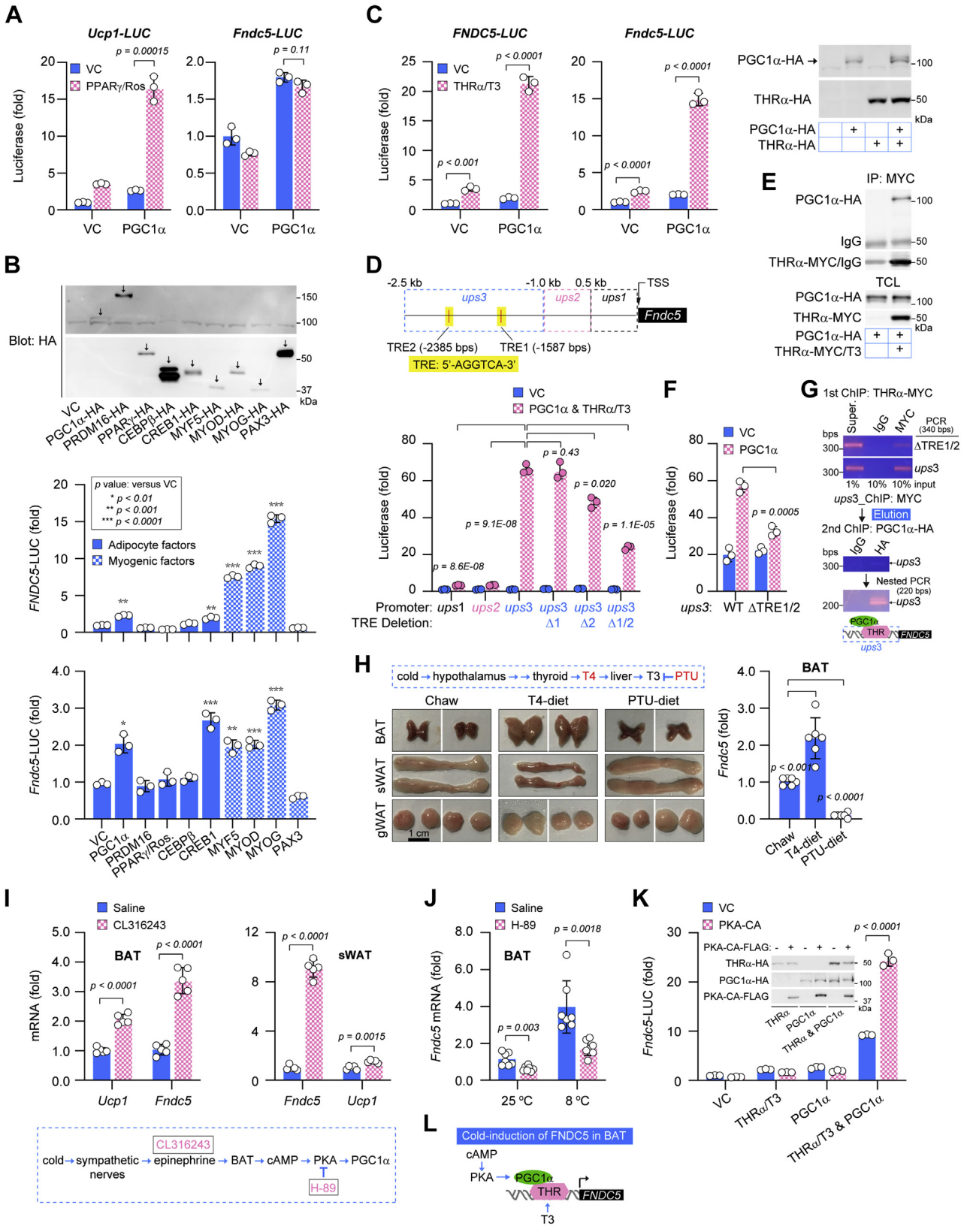

Figure 2. PGC1α and thyroid hormone receptors (THRs) cooperate to facilitate *FNDC5* gene promoter. *A*, the activation of murine *Fndc5* and *Ucp1* gene promoters regulated by PGC1α and PPARγ in the presence of rosiglitazone (1 μM). n = 3 biological replicates. *B*, the activation of human *FNDC5* (*upper chart*) and murine *Fndc5* (*lower chart*) gene promoters regulated by the adipocyte and myogenic factors. n = 3 biological replicates. The inserted Western blotting examination showing expressions of the transcriptional factors in the reporter assays. *C*, the activation of human *FNDC5* and murine *Fndc5* gene promoters regulated by PGC1α and THRα in the presence of triiodothyronine (T3, 10 nM). n = 3 biological replicates. The inserted Western blotting examination showing expressions of PGC1α and THRα in the reporter assays. *D*, the activation of upstream promoter sequence of the murine *Fndc5* gene promoter regulated by PGC1α and THRα in the presence of T3 (10 nM). n = 3 biological replicates. The inserted schematic diagram shows *ups1*, *ups2*, and

active SRC (Y530F) cannot interfere with RUNX2 transactivation (Fig. 3, *G* and *H*). Hence, we conclude that FAK may facilitate the FNDC5/irisin signaling independently of SRC kinase.

WWP2-mediated RUNX2 activation is required for FNDC5/irisin–FAK signaling

We had demonstrated that the monoubiquitination catalyzed by E3 ubiquitin–protein ligase. WWP2 can facilitate RUNX2 transactivation (35). Here, we identified that FAK can bind and phosphorylate WWP2 (Fig. 4, *A* and *B*). Irisin cannot regulate the interaction of FAK and WWP2 (Fig. 4*C*) but promote FAK-catalyzed WWP2 tyrosine phosphorylation (Fig. 4*D*). Moreover, constitutively active FAK-K38A significantly enhances WWP2 self-ubiquitination as well as WWP2-mediated RUNX2 ubiquitination (Fig. 4, *E* and *F*). Taken together, the results suggest that E3 ubiquitin–protein ligase WWP2 may mediate the regulation of FNDC5/irisin–FAK signaling axis in RUNX2 transactivation. Consistent with these findings, irisin and WWP2 cooperate to promote RUNX2 transactivation in an FAK-dependent manner (Fig. 4*G*), and reduction in WWP2 expression significantly inhibits the irisin-stimulated RUNX2 transactivation (Fig. 4*H*). We previously identified that the substitutions of Lys-202 and Lys-225 (K202/225R) in RUNX2 proteins abolished WWP2-catalyzed RUNX2 ubiquitination (35). Such substitutions also inhibit irisin-mediated RUNX2 transactivation (Fig. 4*I*). Collectively, the results support that WWP2-catalyzed ubiquination is required for FNDC5/irisin signaling to facilitate RUNX2 transactivation.

FNDC5/irisin signaling activates RUNX1/2 in the subcutaneous WAT

As a target of RUNX2, the *Ocn* gene was observed to be preferentially expressed in the subcutaneous WAT as compared with that in visceral WAT or scapular BAT (Fig. 5*A*), and moreover, its expression can be stimulated by long-term cold exposure lasting at 1 day (Fig. 5*B*). Similarly, long-term instead of acute cold exposure induces FNDC5 expression in the BAT (Fig. 5*C*). Interestingly, perturbation of FNDC5/irisin signaling by treatment of FAK inhibitor PF562271 not only suppressed cold-induced "browning" of subcutaneous WAT but also attenuated the expression of *Ocn* as well as thermogenesis genes (Fig. 5*D*). Moreover, knockdown of WWP2 also attenuated *Ocn* gene expression in the subcutaneous WAT (Fig. 5*E*). Hence, the results indicate that the expression of *Ocn* gene in subcutaneous WAT may be regulated by FNDC5/irisin signaling. In order to further confirm such regulation of FNDC5/irisin signaling, the inguinal WATs were cultured *in vitro* and stimulated by the conditioned medium containing the s-Irisin peptide for 24 h (Fig. 5*F*). We observed that the s-Irisin conditioned medium stimulates both *Ucp1* and *Ocn* genes in an FAK-dependent manner while the treatment of β3-AR agonist CL316243 only stimulated *Ucp1* gene (Fig. 5*F*), supporting that FNDC5/irisin signaling can directly activate the *Ocn* gene in the subcutaneous WAT.

There exists three RUNX1–3. Among them, RUNX1 and RUNX2 were abundant in preadipocytes such as immortalized 3T3-L1 cells as well as ADSCs isolated from subcutaneous inguinal WAT (Fig. 5, *G* and *H*). Interestingly, the mRNA levels of *Runx1* and *Runx2* in subcutaneous WAT are significantly higher than that in visceral WAT or scapular BAT (Fig. 5, *I* and *J*). We confirmed that FAK similarly facilitates WWP2-catalyzed RUNX1 ubiquitination (Fig. 5*K*) and that the hormone-like irisin potentiates RUNX1 transactivation on *Ocn* gene promoter (Fig. 5*L*). Therefore, we speculate that RUNX1/2 may be responsible for *Ocn* gene activation in the subcutaneous WAT. The RUNXs harbor a runt domain responsible for DNA binding. Ectopic expression of the runt homology domain (RHD) derived from RUNX2 is capable of competing with RUNX1/2 in 3T3-L1 cells, thereby leading to significant inhibition of *Ocn* gene expression activated by RUNX1/2 (Fig. 5*M*). We then forced RHD expression in the subcutaneous inguinal WAT of 6-week mice, and the inguinal WATs harboring RHD expression were cultured *in vitro* in the presence of s-Irisin conditioned medium or β3-AR agonist CL316243. The *Ocn* gene in cultured WAT could be specifically activated by hormone-like irisin peptides, but the activation was significantly suppressed by the forced expression of RHD as expected (Fig. 5*N*). Given these findings, we suggest that the RUNX1/2 can be activated by FNDC5/irisin signaling in the subcutaneous WAT.

RUNX1/2 is involved in browning of the subcutaneous WAT

In addition to *Ocn* gene, forced expression of RHD in subcutaneous inguinal WAT also suppressed the expression of cold-induced thermogenesis-related genes, such as *Ucp1* and

ups3 promoter of *Fndc5* gene. TRE, THR-binding elements; Δ1, TRE1 deletion; Δ2, TRE2 deletion; Δ1/2, TRE1 and TRE2 deletion. *E*, coimmunoprecipitation of PGC1α with THRα in the presence of T3 (10 nM) in HEK293T cells. *F*, TRE deletions suppress PGC1α-activated *ups3* promoter of the murine *Fndc5* gene. n = 3 biological replicates. *G*, re-ChIP assays confirm the colocalization of PGC1α and THRα on the *ups3* promoter of the murine *Fndc5* gene. The upper agarose gels showing PCR examinations of *ups3* and *ups3*-ΔTRE1/2 promoters in ChIP complexes, and the lower agarose gel showing nested PCR examinations of *ups3* promoter in re-ChIP complexes. *H*, 8-week-old mice were fed with thyroxine (T4, n = 6 mice) or propylthiouracil (PTU, n = 6 mice) for 2 weeks. The scapular BAT, subcutaneous WAT (sWAT), and gonadal WAT (gWAT) were shown, and the inserted graphic chart showed *Fndc5* mRNA levels in BAT. *I*, *Fndc5* and *Ucp1* mRNA levels in scapular BAT and subcutaneous WAT were affected by intraperitoneal injection of CL316243 (0.5 mg/kg/day, n = 6 mice) for 3 days and saline (0.9% NaCl, n = 6 mice) as controls. *J*, *Fndc5* mRNA levels in scapular BAT were affected by intraperitoneal injection of H-89 (50 mg/kg/day) for 3 days and saline (0.9% NaCl) as controls. The mice were divided into two groups, the room temperature group housed at 25 °C (n = 7 mice) and the cool group housed at 8 °C (n = 7 mice). *K*, the activation of *Fndc5* gene promoter regulated by PKA catalytic subunit (PKA-CA), PGC1α, and THRα (T3, 10 nM). n = 3 biological replicates. The inserted Western blotting examination showing expressions of PGC1α, THRα, and PKA-CA in the reporter assays. *L*, the schematic diagram showing the activation of *Fndc5* gene promoter in BAT in response to cold exposure. (All data are shown as the average values ± SD, two-tailed Student's *t* test was applied in *A–D*, *F*, *G*, and *K*, and two-tailed ANOVA test was applied in *H–J*.). FNDC5, fibronectin type III domain–containing protein 5; HEK293T, human embryonic kidney 293T cell line; PGC1α, peroxisome proliferator–activated receptor γ coactivator-1α; PPARγ, peroxisome proliferator–activated receptor γ.

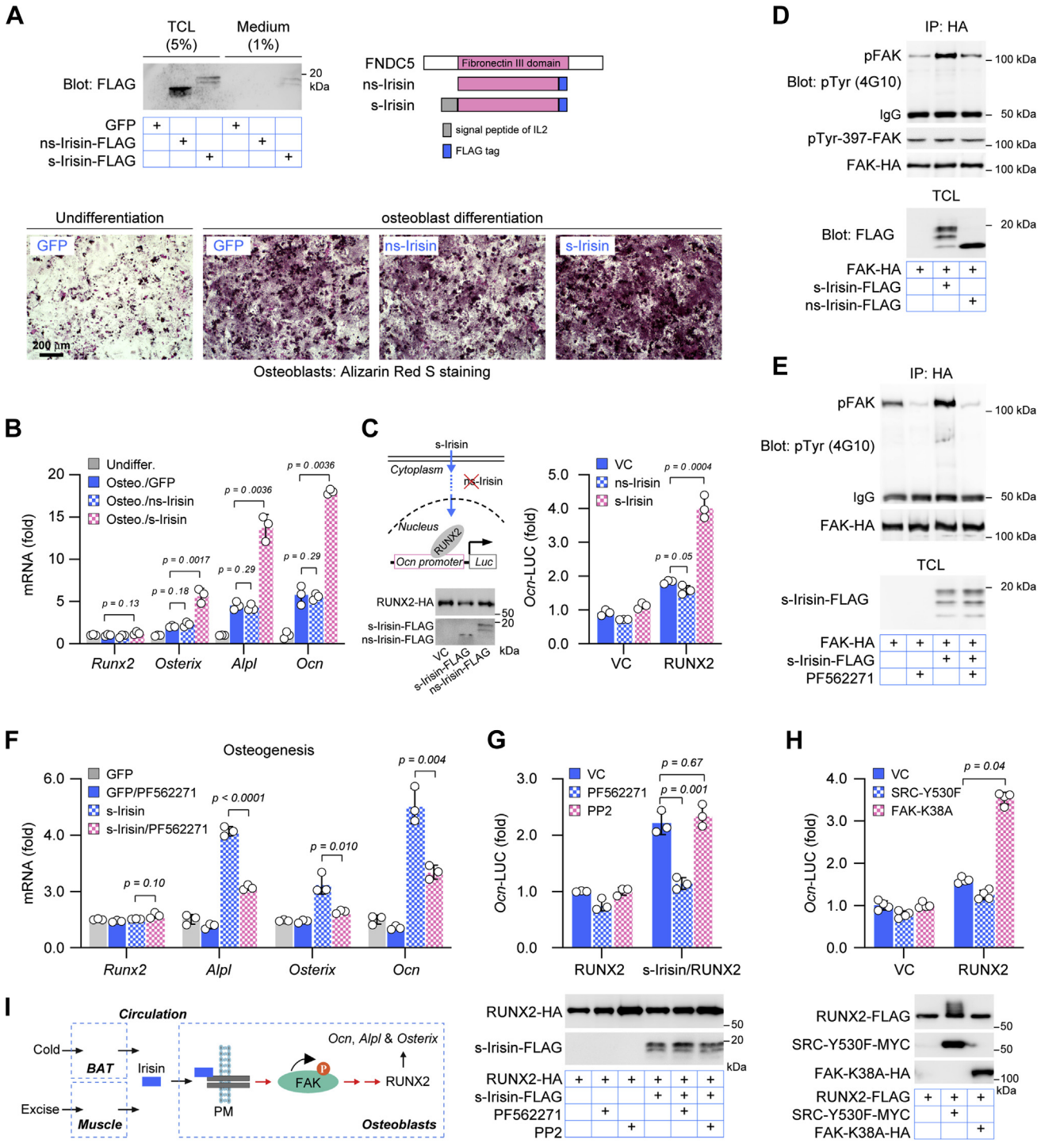

Figure 3. FNDC5/irisin stimulates the runt-related transcriptional factor 2 (RUNX2) in osteoblasts. *A*, the secreted (s) and nonsecreted (ns) irisin peptides derived from murine FNDC5 as indicated were ectopically expressed in primary osteoblasts, which were then subjected into osteoblast differentiation. The irisin expressed in osteoblasts and secreted in culture medium was examined. For Western blotting, 5% of the total cell lysates (TCLs) and 1% of the culture medium were employed. Staining of Alizarin Red S showed mineral deposition during osteoblast differentiation. *B*, the primary osteoblasts ectopically expressing GFP, ns-Irisin, or hormone-like irisin (s-Irisin) underwent osteogenesis *in vitro*. The analysis of quantitative RT–PCR determined the activation of osteoblast genes, n = 3 biological replicates. *C*, s-Irisin stimulates transactivation of RUNX2 on the *Ocn* gene promoter, n = 3 biological replicates. The inserted Western blotting examination showing expressions of RUNX2, s-Irisin, and ns-Irisin in the reporter assays. *D*, the s-Irisin stimulates FAK tyrosine phosphorylation. FAK was coexpressed with s-Irisin or ns-Irisin in HEK293T cells for 24 h, then FAK proteins were pulled down and examined by a pan phosphotyrosine (4G10) or a specific Tyr-397 phosphorylation antibody. *E*, the s-Irisin stimulates FAK tyrosine phosphorylation that is inhibited by FAK inhibitor PF562271 (1 μM). *F*, the s-Irisin stimulates osteoblast genes during osteoblast differentiation *in vitro* in the absence or the presence of FAK inhibitor PF562271 (1 μM), n = 3 biological replicates. *G*, the s-Irisin stimulates transactivation of RUNX2 on the *Ocn* gene promoter in the presence of FAK inhibitor PF562271 (1 μM) or SRC inhibitor PP2 (5 μM), n = 3 biological replicates. The inserted Western blotting examination showing expressions of RUNX2 and s-Irisin in the reporter assays. *H*, active FAK (K38A) and SRC (Y530F) regulate the transactivation of RUNX2 on the *Ocn* gene promoter, n = 4 biological replicates. The inserted Western blotting examination showing expressions of RUNX2, SRC (Y530F), and FAK (K38A) in the reporter assays. *I*, the schematic diagram shows communications between cold-activated BAT and bone formation. (All data are shown as the average values ± SD, two-tailed Student's

Cidea (Fig. 6*A*). At the same time, the brown-like conversion of inguinal WAT was significantly damaged (Fig. 6*B*). In order to further explore RUNX1/2 regulation in the subcutaneous WAT, we performed a size-exclusion chromatography to analyze the endogenous protein complexes containing RUNX1/2 in the inguinal WATs. The protein complexes from the inguinal WAT were collected according to their whole molecular weights, and PRDM16 that is a transcriptional coactivator crucial for "browning" of the subcutaneous WAT (36) was enriched together with RUNX1/2 in an elution of high molecular weight (Fig. 6*C*). Importantly, we verified that RUNX2 interacted with PRDM16 in a WWP2-dependent manner and further found that the double mutations (K202/225R) abolishing WWP2-catalyzed RUNX2 ubiquitination attenuated the protein interaction of RUNX2 and PRDM16 (Fig. 6*D*). In addition, the protein interaction of PRDM16 and RUNX1 was also mediated by WWP2 (Fig. 6*E*). Notably, WWP2 can also bind PRDM16, and the interaction can be promoted by irisin (Fig. 6*F*), and the WWP2 protein will be transported into the nucleus during adipogenesis (Fig. 6*G*). Therefore, we demonstrate that WWP2 may mediate the transcriptional machinery composed of RUNX1/2 and PRDM16 in the subcutaneous WAT. On the chromatin DNA upstream of the *Ucp1* gene promoter, there are multiple runt domain–recognized DNA consensus sequences. Consistent with these findings, we detected the enrichment of RUNX2 proteins on the distal region upstream of *Ucp1* gene promoter (Fig. 6*H*).

Although current evidence extensively demonstrates physiological relevance of FNDC5/irisin in metabolic and skeletal homeostasis (8–10, 16), knowledge about molecular mechanism underlying its regulation still remains limited. Overall, our presented data illustrate a novel signaling axis facilitated by FNDC5/irisin and provide a better understanding about the molecular mechanism underlying multifaceted interorgan communications in the muscle–adipose–bone connectivity (Fig. 7).

Discussion

Impaired expression of FNDC5/irisin is not only associated with obesity and type 2 diabetes (8–15) but also with the risk of osteoporosis in patients with metabolic disorders (10, 16–21). However, how the *FNDC5* gene is transcriptionally controlled and how FNDC5/irisin regulates metabolic and skeletal homeostasis, thereby establishing the muscle–adipose–bone connectivity, are still largely unknown. Here, we found that FNDC5 can be expressed in cold-stimulated BAT and further showed the FNDC5 gene promoter is under the cooperative control of PGC1α and thyroxine receptor THRs. Downstream of FNDC5/irisin, we established the FAK–WWP2–RUNX1/2 axis to control the gene expression related to bone remodeling as well as subcutaneous WAT thermogenesis and further revealed that the transcriptional coactivator PRDM16 is complex with RUNX1/2 in a ubiquitination-dependent manner. Therefore, the findings clarify the FNDC5/irisin-implicated signaling mechanisms in the interorgan communications of muscle, BAT, and bone.

FNDC5/irisin is generally considered as a myokine, but current evidence indicates that it may also be an adipokine. Circulating irisin concentration was showed to be positively associated with body mass index or obesity in humans (37–40). Moreover, the irisin level measured in adipose tissue extraction was strongly associated with *FNDC5* gene transcription in both subcutaneous and visceral WAT (41). However, the expression of FNDC5 in human subcutaneous WAT is 100 folds lower than that in skeletal muscle (41). Here, we demonstrate that the *FNDC5* gene can be activated during brown fat differentiation and is preferentially expressed in BAT, in which FNDC5 expression is elevated by 10 folds than in subcutaneous WAT. Unlike WAT, BAT and skeletal muscle are both derived from MYF5-positive precursor cells (42). This may cause predominant expression of FNDC5 in BAT rather than WAT. However, the expression of FNDC5 in BAT cannot be activated by exercise but activated by cold exposure, which further lead to approximately fivefold increase in FNDC5 expression in BAT. Although cold exposure induces "browning" of subcutaneous WAT, it fails to facilitate FNDC5/irisin in subcutaneous WAT. In addition, we confirmed that cold exposure cannot promote the expression of FNDC5/irisin in skeletal muscle, as well as heart, liver, brain, and so on. Therefore, BAT is a specific tissue that facilitates the expression of FNDC5/irisin in response to cold stimulation. A previous report has indicated that cold exposure increased circulating irisin concentration in humans and suggested that the increased irisin concentration is associated with shivering-related muscle contraction (43). We observed that cold-induced expression of FNDC5 in BAT doubled in mice undergoing free-wheel exercise, confirming that muscle contraction is beneficial to the expression of FNDC5/irisin in BAT.

Although FNDC5 was revealed to be transcriptionally controlled by PGC1α (8), its promoter can only moderately activated by PGC1α. At the same time, the modulation of PGC1α on the *FNDC5* gene promoter cannot be promoted by its classic coactivator PPARγ. Our results indicate that the THRs are copartners of PGC1α in BAT, and it can cooperate with PGC1α to activate the *FNDC5* gene promoter. PGC1α interacts with THR and is colocalized with THR on the upstream promoter of the *FNDC5* gene. Therefore, cold exposure promotes activation of THRs and PGC1α in BAT *via* thyroxine and adrenaline signaling, culminating in *FNDC5* gene activation. In addition, we also identified multiple myogenic factors, which have capability to activate the *FNDC5* gene promoter, but they cannot cooperate with PGC1α on the *FNDC5* gene promoter, indicating that there may exist distinct

t test was applied in *C*, *G*, and *H*, and two-tailed ANOVA test was applied in *B* and *F*.). BAT, brown adipose tissue; FAK, focal adhesion kinase; FNDC5, fibronectin type III domain–containing protein 5; HEK293T, human embryonic kidney 293T cell line; Osteo., osteoblast differentiation; Undiffer., undifferentiaiton.

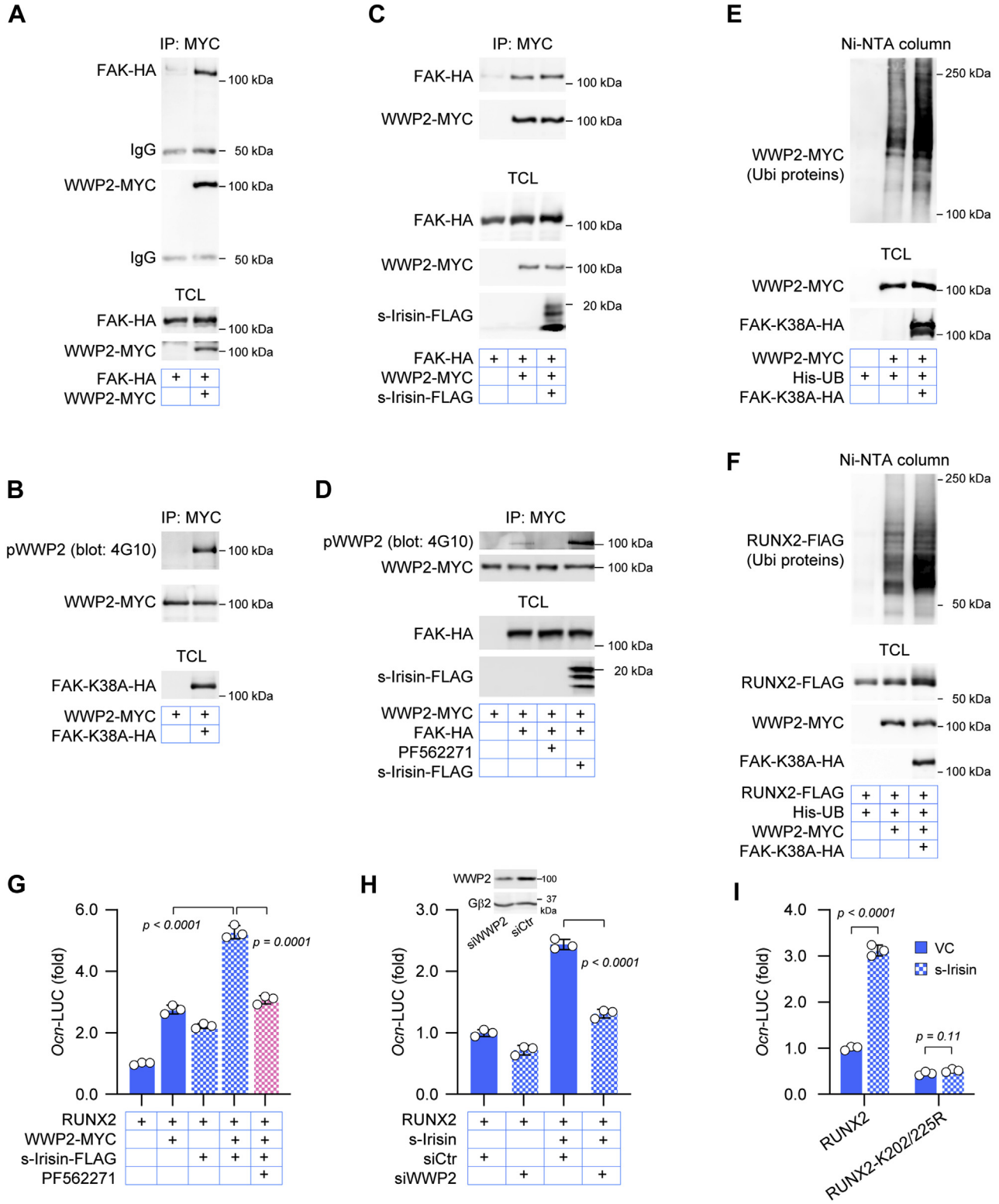

Figure 4. WWP2-mediated RUNX2 activation is required for FNDC5/irisin–FAK signaling. *A*, coimmunoprecipitation of FAK with WWP2 in HEK293T cells. *B*, active FAK (K38A) catalyzes WWP2 tyrosine phosphorylation. WWP2 was coexpressed with FAK-K38A in HEK293T cells for 24 h, then WWP2 proteins were pulled down and examined by a pan phosphotyrosine antibody (4G10). *C*, the secreted irisin (s-Irisin) does not stimulate protein interaction of FAK and WWP2. *D*, the s-Irisin stimulates FAK to phosphorylate WWP2. PF562271, 1 μM. *E*, active FAK (K38A) enhances WWP2 self-ubiquitination. *F*, active FAK (K38A) enhances WWP2-catalyzed RUNX2 ubiquitination. *G*, the s-Irisin depends on FAK to stimulate WWP2-mediated RUNX2 transactivation on the *Ocn* gene promoter. PF562271, 1 μM, n = 3 biological replicates. *H*, the s-Irisin depends on WWP2 to stimulate RUNX2 transactivation on the *Ocn* gene promoter, n = 3 biological replicates. The Western blotting examination indicated siRNA-mediated knockdown of WWP2. *I*, the substitution of K202 and K225 on RUNX2 protein inhibited s-Irisin regulation in RUNX2 transactivation on the *Ocn* gene promoter, n = 3 biological replicates. (All data are shown as the average values ± SD, two-tailed Student's *t* test was applied in *G*–*I*.). FAK, focal adhesion kinase; FNDC5, fibronectin type III domain–containing protein 5; HEK293T, human embryonic kidney 293T cell line; RUNX2, runt-related transcriptional factor 2; WWP2, WW domain–containing protein 2.

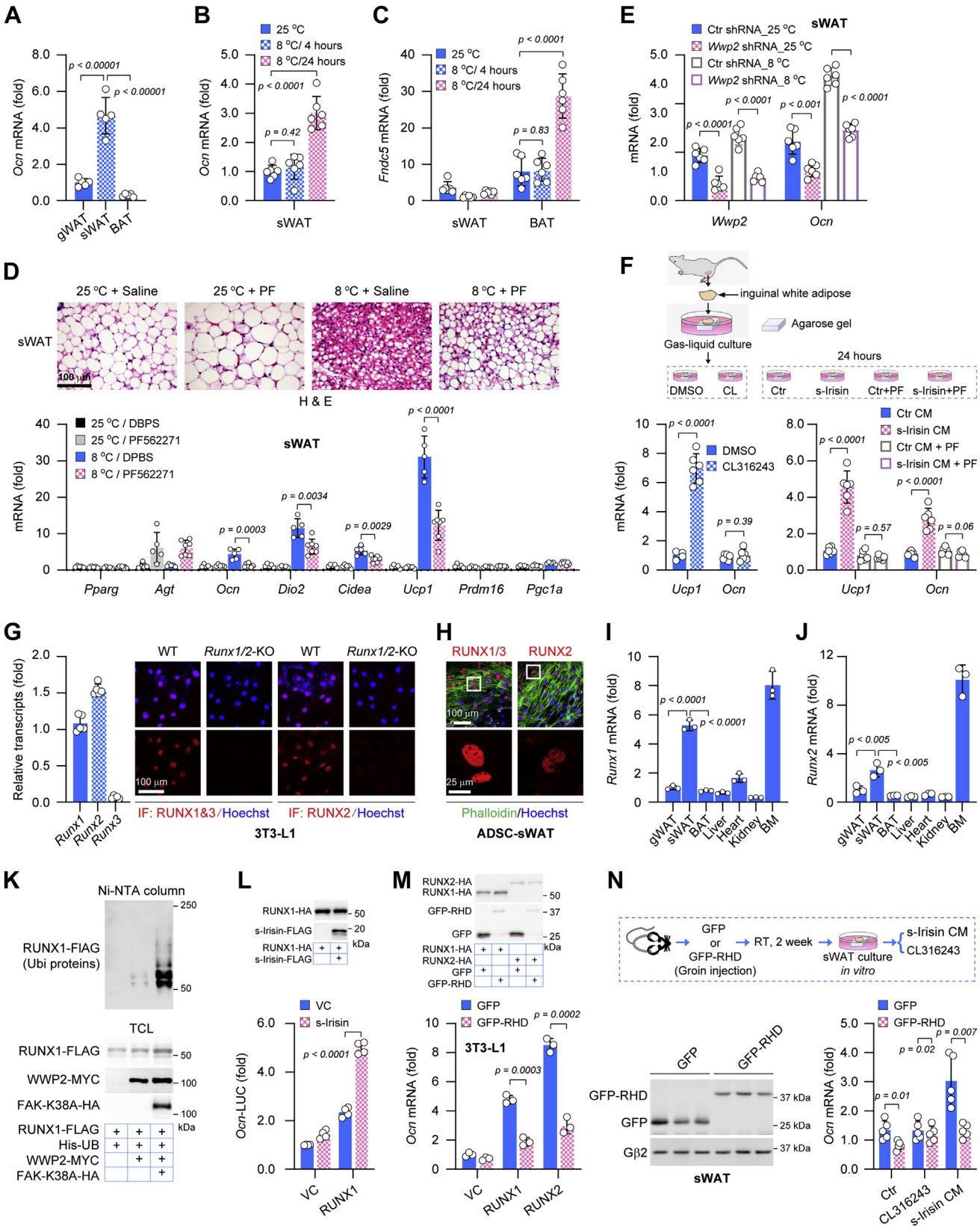

Figure 5. FNDC5/irisin signaling activates RUNX1/2 in the subcutaneous WAT (sWAT). *A*, *Ocn* mRNA levels in gonadal WAT (gWAT), sWAT, and scapular BAT, n = 5 mice. *B*, *Ocn* mRNA levels in sWAT that was activated by cold exposure for 4 h or 24 h, n = 6 mice. *C*, *Fndc5* mRNA levels in sWAT and scapular BAT that were activated by cold exposure for 4 h or 24 h, n = 6 mice. *D*, saline (0.9% NaCl) or PF562271 (5 mg/kg/day) was injected into the groin of 6-week-old mice for 6 days. From the day 4 to day 6, mice were housed at room temperature (n = 5 mice) or 8 °C (n = 7 mice), histological hematoxylin–eosin staining to show "browning" of sWAT (*the upper panel*), and quantitative RT–PCR examination for expression of *Ocn* and thermogenesis genes (*the graphic chart*). *E*, lentiviruses carrying scramble or *Wwp2* shRNA were injected into the groin of 6-week-old mice. After 1 week, mice were housed at room temperature

transcriptional machineries implicated in FNDC5 expression in skeletal muscle.

FNDC5/irisin stimulates WAT to adopt a BAT-like phenotype *via* increasing mitochondrial biosynthesis and UCP1 expression, thus leading to expenditure of excessive energy intake (8). However, loss of FNDC5/irisin in mice showed normal body weight but reduced bone formation (10), indicating that low-level expression of FNDC5/irisin in sedentary condition may participate in bone formation instead of WAT "browning." The dose of recombinant irisin administrated to healthy mice for promoting bone formation was 35-folds lower than the dose for WAT "browning." Therefore, the primary target organ of FNDC5/irisin may be the skeleton rather than WAT (16). The active BAT helps to maintain the normal body temperature in newborns and infants but not in the adults. Although the existence of active BAT in healthy adult humans has been confirmed (1, 2), the limited size leads to a debate about its physiological significance in energy metabolic homeostasis of adults. Cold-activated BAT not only facilitates energy metabolism but also benefits femoral bone structure and bone mineral density, although the mechanism is unclear (29–31). We confirmed that although the reduction of FNDC5 expression does not affect the differentiation of brown preadipocytes (data not shown), interfering with the expression of FNDC5/irisin in BAT-attenuated cold-induced expression OCN in bone. Therefore, BAT in adults may not act as the substantial metabolic organ but instead as a key paracrine tissue producing various adipokines such as FNDC5/irisin to facilitate interorgan communications in metabolic and skeletal homeostasis.

The RUNXs are characterized as the evolutionarily conserved RHD that is a 128-amino-acid region mediating DNA binding (44). RUNX1 is required for hematopoietic cell differentiation, whereas RUNX2 promotes osteoblast differentiation and chondrocyte maturation during skeletal development (45, 46). Interestingly, RUNX1 and RUNX2 were also detected in various adipocyte progenitors as well as the subcutaneous WAT. We had demonstrated that E3 ubiquitin–protein ligase WWP2 facilitates RUNX2 transactivation during osteoblast differentiation *via* catalyzing nonproteolytic monoubiquitination (35). Here, we found that FNDC5/irisin is capable of activating FAK *via* SRC-independent pathway and that the active FAK enhances WWP2-mediated ubiquitination of RUNX1/2. Unexpectedly, the transactivation of the RUNXs not only exists in osteoblast differentiation but also emerges in "browning" of subcutaneous WAT, where it mediates FNDC5/irisin signaling. Several lines of evidence demonstrate a putative regulation of RUNX1/2 in subcutaneous WAT. First, like themselves, their target gene *Ocn* is also preferentially expressed in subcutaneous WAT and is regulated by the FNDC5/irisin–FAK–WWP2 signaling axis. Interfering with the DNA-binding activity of RUNX1/2 in subcutaneous WAT attenuated *Ocn* gene expression. Second, competitive inhibition of RUNX1/2 DNA binding results in damage to brown fat–like conversion of subcutaneous WAT as well as the expression of *UCP1* gene. Third, the enrichment of the RUNX family proteins is detected on the chromatin DNA flanking *Ucp1* gene promoter. Finally, the RUNX family proteins can be complex with PRDM16, which is the core transcriptional coactivator for the brown fat–like conversion of subcutaneous WAT (36).

RUNX2 and WWP2 have been implicated in craniofacial skeleton development (46–48). We had uncovered three lysine residues on mouse Runx2 proteins, K202, K225, and K240, which are required for WWP2-prompted RUNX2 ubiquitination and transcriptional activity (35), and moreover, somatic mutations in these lysine residues had been found to be associated with cleidocranial dysplasia (49). Notably, PRDM16 depletion in mice also causes the defects of craniofacial skeleton development (36, 50). We confirmed that substitution of these lysine residues in RUNX2 could abolish the protein interaction of RUNX2 and PRDM16 and the regulation of FNDC5/irisin in RUNX2 transactivation. Therefore, the findings further indicate that the FNDC5/irisin–FAK–WWP2 signaling axis may also function in chondrocytes *via* promoting the formation of RUNX2 and PRDM16 transcriptional machinery. Consistent with these findings, treatment of irisin stimulates proliferation and anabolism of human osteoarthritic chondrocytes and provides cartilage protection (51, 52).

A large number of evidence has demonstrated that FNDC5/irisin facilitates interorgan communications between skeletal muscle, adipose, and bone. However, a comprehensive understanding of the molecular mechanisms underlying FNDC5/irisin regulation is still an issue. In the present study, we uncovered a key role of FNDC5/irisin in the paracrine function of BAT in response to cold stimulation and linked the RUNXs to FNDC5/irisin regulation in both the osteoblast differentiation

(n = 6 mice) or 8 °C (n = 6 mice) for 1 week. The mRNA levels of *Ocn* and *Wwp2* in sWAT were measured. *F*, the fresh subcutaneous inguinal WAT was cultured *in vitro* on the agarose gel blocks that were half immersed in the culture medium as indicated. After 24 h, the mRNA levels of *Ocn* and *Ucp1* in cultured WAT were measured (n = 6 cultures). CM, conditioned medium; CL316243, 1 μM; PF, PF562271, 1 μM. *G*, the *graphic chart* showed relative transcript numbers of *runx1–3* in 3T3-L1 preadipocytes. For standard curves in the quantitative RT–PCR analyses, plasmids containing murine *Runx*1–3 cDNA (1, 10^{-1}, 10^{-2}, 10^{-3}, 10^{-4}, 10^{-5}, and 10^{-6} ng) were employed. n = 3 technical replicates. Immunofluorescences against RUNX1/3 and RUNX2 were performed in WT and *Runx1/2* double knockout (*Runx1/2*-KO) 3T3-L1 preadipocytes. Knockout of *Runx1* gene that abolished the staining of RUNX1/3 antibodies suggests that there is only RUNX1 expression in 3T3-L1 cells. *H*, immunofluorescences against RUNX1/3 and RUNX2 were performed in ADSC derived from WAT. *I*, *Runx1* mRNA levels were examined in various mouse tissues, n = *3* mice. *J*, *Runx2* mRNA levels were examined in various mouse tissues, n = 3 mice. *K*, active FAK (K38A) enhances WWP2-catalyzed RUNX1 ubiquitination. *L*, the secreted irisin (s-Irisin) stimulates transactivation of RUNX1 on the *Ocn* gene promoter, n = 3 biological replicates. The inserted Western blotting examination showing expressions of RUNX1 and s-Irisin in the reporter assays. *M*, RHD blocks RUNX1/2-activated *Ocn* gene expression in 3T3-L1 preadipocytes, n = 3 biological replicates. The inserted Western blotting examination showing expressions of RUNX1, RUNX2, and GFP-RHD in the reporter assays. *N*, lentiviruses expressing GFP or RHD-GFP were injected into the groin of 6-week-old mice for 2 weeks, then fresh subcutaneous inguinal WAT was cultured *in vitro* as stimulated by s-Irisin conditioned medium or CL316243 for 24 h, n = 5 mice. The Western blotting examination showing expressions of GFP or GFP-RHD in cultured WAT, and the graphic chart showed *Ocn* gene expression in WAT. (All data are shown as the average values ± SD, two-tailed Student's *t* test was applied in *G*, *I*, *J*, *L*, and *M*, and two-tailed ANOVA test was applied in *A–F* and *N*.). BAT, *brown adipose* tissue; cDNA, complementary DNA; FAK, focal adhesion kinase; FNDC5, fibronectin type III domain–containing protein 5; RHD, runt homology domain; RUNX1/2, runt-related transcriptional factors 1/2; WAT, white adipose tissue; WWP2, WW domain–containing protein 2.

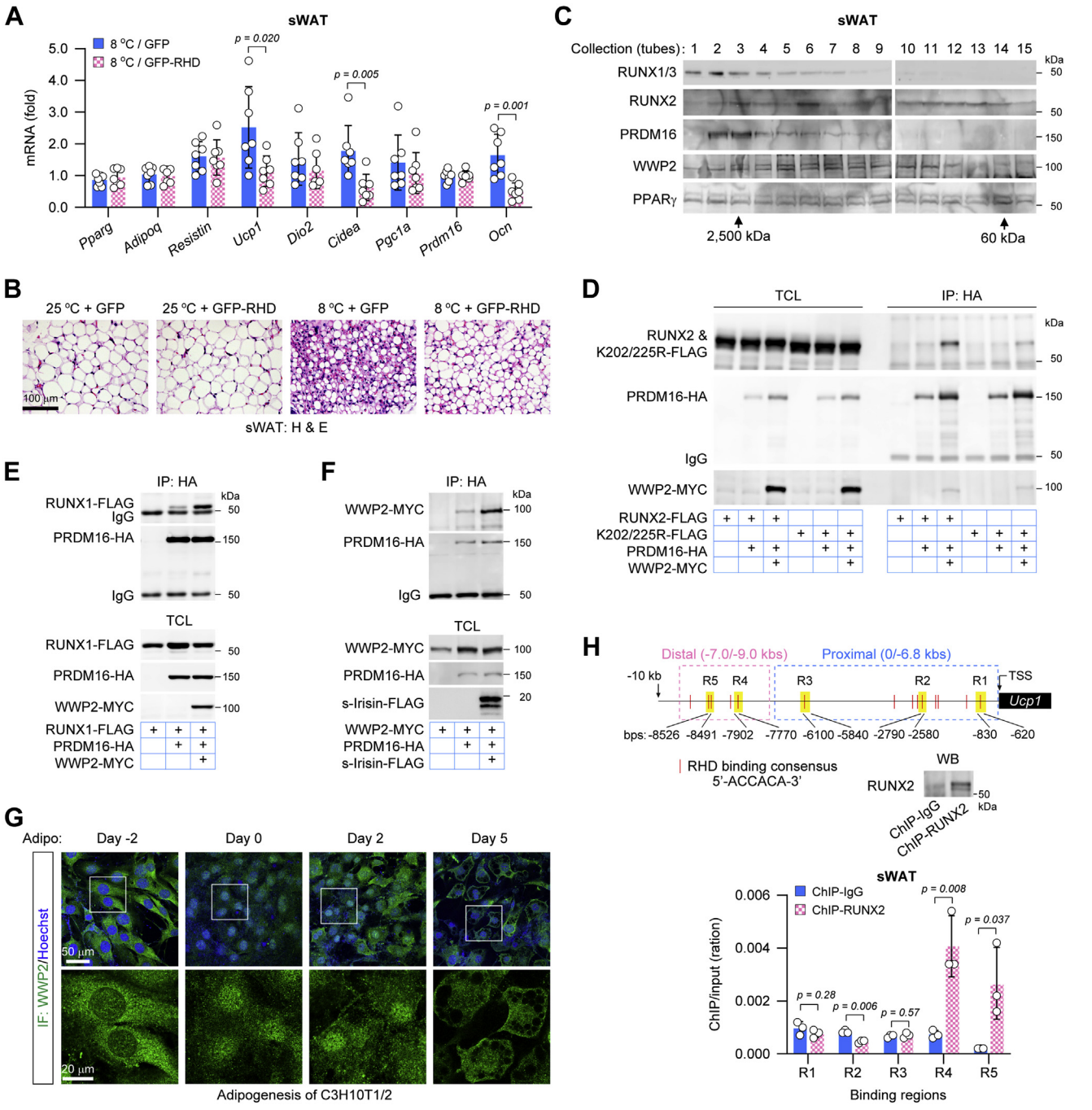

Figure 6. RUNX1/2 is involved in browning of the subcutaneous WAT. *A* and *B*, lentiviruses expressing GFP or RHD-GFP were injected into the groin of 6-week-old mice for 2 weeks, then mice were housed at room temperature (n = 7 mice) or 8 °C (n = 7 mice) for 1 week. Inguinal WAT depots were subjected to quantitative RT–PCR examination (*A*) and histological hematoxylin–eosin staining (*B*). *C*, the size-exclusion chromatography assay of endogenous protein complexes in mouse inguinal WAT depots. The protein complexes were collected according to their molecular weight using a Superose 6 10/300 GL column on a fast protein liquid chromatography (FPLC), and then the components in each collection tube were checked by Western blotting. The numbers represent the collection order. *D*, WWP2 mediates the protein interaction of PRDM16 with RUNX2 or RUNX2-K202/225R. *E*, WWP2 promotes the protein interaction of PRDM16 with RUNX1. *F*, s-Irisin stimulates the protein interaction of PRDM16 with WWP2. *G*, immunofluorescences against WWP2 proteins were performed during adipogenesis of C3H10T1/2 cells. Day −2, 0, 2, and 5 represented differentiation time. *H*, the quantitative PCR examinations showed the enrichment of RUNX2 on the promoter and enhancer of *Ucp1* gene, n = 3 technical replicates. The inserted schematic diagram shows RHD binding consensus 5′-ACCACA-3′ on the chromatin DNA adjacent to *Ucp1* gene. Chromatin immunoprecipitation (ChIP) was performed in mouse subcutaneous inguinal WAT depots. The Western blotting examination showed that RUNX2 protein pulled down by ChIP assays. (All data are shown as the average values ± SD; two-tailed ANOVA test was applied in *A* and *H*.). PRDM16, PR domain–containing protein 16; RHD, runt homology domain; RUNX1/2, runt-related transcriptional factors 1/2; s-Irisin, secrered irisin; *Ucp1*, uncoupling protein 1; WAT, white adipose tissue; WWP2, WW domain–containing protein 2.

and the brown fat–like conversion of subcutaneous WAT, thereby providing a novel insight into the maintenance of metabolic and skeletal homeostasis (Fig. 7). It is worth noting that FNDC5/irisin was reported to be positively correlated with circulating uncarboxylated OCN, which is derived from bone matrix and functions as the bone hormone implicated in

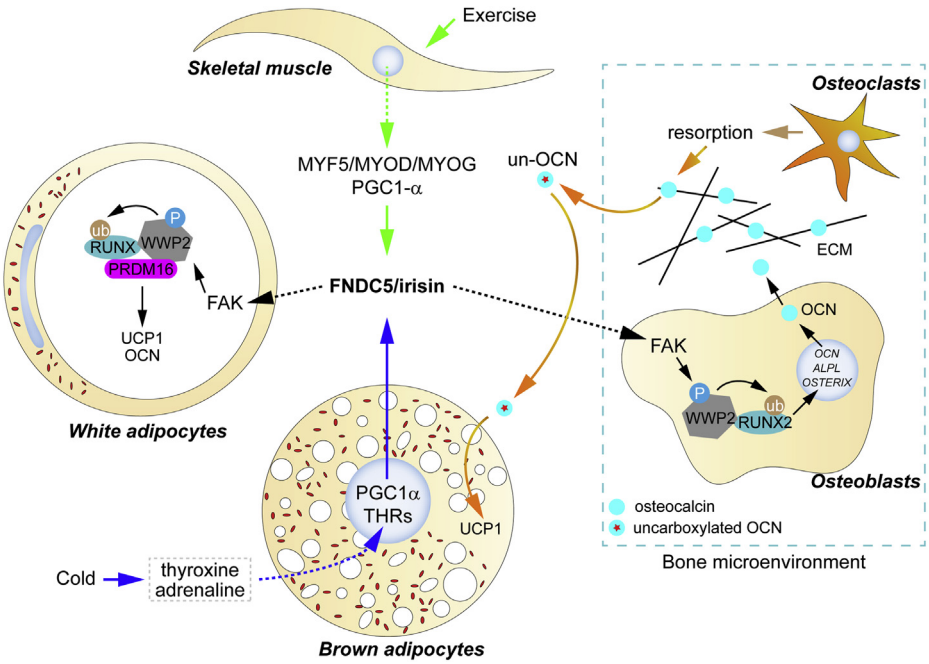

Figure 7. Schematic diagram for multifaced interorgan communications regulated by FNDC5/irisin signaling in muscle–adipose–bone connectivity. In brief, exercise and cold stimulation promote the expression of FNDC5/irisin in skeletal muscles and brown adipocytes, respectively. Hormone-like irisin can induce WWP2-facilitated RUNX1/2 transactivation through FAK-mediated signaling, leading to activation of osteoblast genes such as *OCN*, *ALPL*, and *OSTERIX* during bone remodeling as well as thermogenesis gene *UCP1* in "browning" of white adipocytes. As a positive feedback, the noncarboxylated osteocalcin is released from bone extracellular matrix into the circulating irisin concentration during bone resorption stimulating *UCP1* gene activation in brown adipocytes (7). FAK, focal adhesion kinase; FNDC5, fibronectin type III domain–containing protein 5; RUNX1/2, runt-related transcriptional factors 1/2; UCP1, uncoupling protein 1; WWP2, WW domain–containing protein 2.

energy metabolism, skeletal muscle function, and brain development (53). Interestingly, we had demonstrated that hormone-like uncarboxylated OCN is capable of stimulating UCP1 expression in BAT *via* crosstalk with the canonical Wnt signaling pathway (7). Here, we evidenced that FNDC5/irisin is capable of activating RUNX2, leading to OCN expression in both osteoblasts and subcutaneous WAT. The findings therefore indicate that there may exist bidirectional regulations in BAT–bone connectivity *via* hormone-like irisin and OCN (Fig. 7).

Experimental procedures

Reagents and antibodies

Protein A/G-PLUS-agarose beads were purchased from Santa Cruz; antibodies to HA.11 (16B12, 1:1000 dilution; catalog no.: 901514) and MYC (9E10, 1:1000 dilution; catalog no.: 626802) from BioLegend; FLAG M2 (1:1000 dilution; catalog no.: F3165) from Sigma–Aldrich; Gβ2 (C-16, 1:1000 dilution; catalog no.: sc-380) and GFP (1:5000 dilution; catalog no.: sc-9996) from Santa Cruz; RUNX2 (mAb D1H7, 1:1000 dilution; catalog no.: 8486), PPARγ (mAb 81B8, 1:1000 dilution; catalog no.:2443) from Cell Signaling; phosphotyrosine (mAb 4G10, 1:1000 dilution; catalog no.: 05-1050) from Millipore; pY397-FAK (1:1000 dilution; catalog no.: ab81298); PRDM16 (1:1000; catalog no.: ab106410), RUNX1/3 (EPR3099; 1:1000 dilution; catalog no.: ab92336), and WWP2 (1:1000 dilution; catalog no.: ab103527) from Abcam.

PF562271 and H-89 from Selleck; CL316243, rosiglitazone, PP2, triiodothyronine (T3), T4 (L-thyroxine), PTU (6-*N*-propyl-2-thiouracil), Oil-Red O, and Alizarin red S from Sigma–Aldrich.

Animals

C57BL/6 mice were from Shanghai Laboratory Animal Center of Chinese Academy of Sciences. All experiments were approved by the Animal Care and Use Committee of the Fudan University Shanghai Medical College. *Lep* gene knockout (*ob/ob*) mice and *Lepr* gene knockout (*db/db*) mice were from ChangZhou Cavens Laboratory Animal Co, Ltd. For cold stimulation, mice were housed in low temperature ambience (8 °C) for indicated time. For athletic stimulation, mice were housed individually in cages with free access to a running wheel, 2 h for each time. Compound CL316243 (0.5 mg/kg/day) and H-89 (50 mg/kg/day) were injected intraperitoneally. Compound PF562271 (5 mg/kg/day) were injected into subcutaneous site adjacent to the inguinal adipose pad. The compound L-thyroxine (T4, 5 mg/kg) and PTU (1.5 g/kg) were spiked into food and fed to mice. To access the "browning" status of inguinal adipose tissues, hematoxylin–eosin staining of paraffin-embedded sections and quantitative RT (qRT)–PCR analysis of thermogenic gene transcription were performed.

Preparation of viruses

Lentiviruses were constructed with pLVX-puro vector (Clontech) for gene expression and pLKO.1 vector (Addgene) for shRNA expression. Viruses were packaged with helper plasmids dR8.9 and VSVG and purified by ultracentrifugation.

For subcutaneous inguinal injection, lentiviruses (5×10^7 of viruses/mouse) were injected into subcutaneous site adjacent to the inguinal adipose pad.

shRNA and siRNA design

The sequences of shRNA targeting the scramble control, *Fndc5*, and *Wwp2* gene were designed as: scramble control, 5′-CCT AAG GTT AAG TCG CCC TCG-3′; *Fndc5*, 5′-AAG ATG GCC TCA AAG AAC AAA-3′; and *Wwp2*, 5′-AAT GGG CGT GTC TAT TAT GTT-3′. The sequences of siRNA targeting the scramble control and *WWP2* gene were designed as: scramble control, TTC TCC GAA CGT GTC ACG T; *WWP2*, 5′-GAG CTT CTC TGG AAT GAG A-3′.

Cell culture

Human embryonic kidney 293T (HEK293T), C3H10T1/2, and 3T3-L1 cells were maintained in Dulbecco's modified Eagle's medium with 10% fetal bovine serum (FBS), 1× GlutaMAX and 1× penicillin–streptomycin solution (Life Technologies), 37 °C, 5% CO_2. The ADSCs of subcutaneous WATs and scapular BATs were isolated from C57BL/6J mice by collagenase digestion as described previously (6, 54) and cultured in α-minimal essential medium with 10% FBS and 1× GlutaMAX, 37 °C, 5% CO_2. Osteoblasts were isolated from long bones of C57BL/6J mice as described (35). Briefly, the bone marrow was flushed out, and then pieces of bone were incubated in collagenase solution at 37 °C, each time for 20 min, repeated four times. Supernatants from the last time of digestion were collected and cultured in α-minimal essential medium with 10% FBS and 1× GlutaMAX, 37 °C, 5% CO_2. *Runx1/2* double knockout 3T3-L1 cells were established by the Cas9–CRISPR method, single-guide RNA targeting *Runx1* gene, 5′-GTC GTT GAA TCT CGC TAC C-3′, and *Runx2* gene, 5′-ACT GTC GGT GCG GAC CAG TT-3′.

Cell transfection and reporter assays

DNAs were transient transfected with Lipofectamine LTX (Life Technologies), and the siRNA was transfected with Lipofectamine RNAiMAX (Life Technologies). The reporter assays were performed 24 h after transfection as described previously (35). For constructions of luciferase reporters driven by murine and human *FNDC5* gene promoters, 2.5 kilobase pairs of the chromatin DNA fragment upstream of the transcription start site were inserted into pGL4.20 (Promega) vector. For luciferase reporter driven by *Ucp1* gene promoters, 6.8 kilobase pairs of the chromatin DNA fragment upstream of the transcription start site were inserted into pGL4.20 vector. For luciferase reporter driven by *Ucp1* gene enhancers, 7.0 to 9.0 kilobase pairs of the chromatin DNA fragment upstream of the transcription start site were inserted into pGL4.20 vector. The luciferase reporter driven by *Ocn* gene promoter was constructed as described previously (35).

Gene transcription analysis

Total RNAs were isolated from tissues using a magnetic bead homogenizer in the TRIzol reagent or from cultured cells by directly adding the TRIzol reagent to the cells. Complementary DNAs (cDNAs) were synthesized using the ProtoScript II, First Strand cDNA Synthesis Kit (BioLabs). qRT–PCR analysis was performed using a Power SYBR Green PCR Master Mix (Life Technologies). 18S RNA levels were used as internal controls in the qPCR analysis. The primers for the qRT–PCR: *18s*, F-5′-CGC CGC TAG AGG TGA AAT TCT-3′, R-5′-CAT TCT TGG CAA ATG CTT TCG-3′; *AdipoQ*, F-5′-GCA CTG GCA AGT TCT ACT GCA A-3′, R-5′-GTA GGT GAA GAG AAC GGC CTT GT-3′; *Agt*, F-5′-GCA CCC TGG TCT CTT TCT ACC-3′, R-5′-TGT GTC CAT CTA GTC GGG AGG-3′; *Alpl*, F-5′-CAT GAG ACC CAC GGT GGA GA-5′, R-5′-CAG GCA CAG TGG TCA AGG TT-3′; *Ocn*, F-5′-CTC TGA CCT CAC AGA TGC CA-3′, R-5′-ACT GGT CTG ATA GCT CGT CA-3′; *Cidea*, F-5′-TGC TCT TCT GTA TCG CCC AGT-3′, R-5′-GCC GTG TTA AGG AAT CTG CTG-3′; *Dio2*, F-5′-AGA GTG GAG GCG CAT GCT-3′, R-5′-GGC ATC TAG GAG GAA GCT GTT-3′; *Fndc5*, F-5′-AGC TGG GAT GTC CTG GAG GA-3′, R-5′-GCA CAT GGA CGA TAT ATT CT-3′; *Osterix*, F-5′-AAA GCA GGC ACA AAG AAG CCG TAC T-3′, R-5′-TGG GAA AAG GGA GGG TAA TCA TTA-3′; *Pgc1a*, F-5′-CCC TGC CAT TGT TAA GAC-3′, R-5′-TGC TGC TGT TCC TGT TTT C-3′; *Pparg*, F-5′-AGA TGA CAG TGA CTT GGC TA-3′, R-5′-GAA CAG CTG AGA GGA CTC TG-3′; *Prdm16*, F-5′-TGG CCT TCA TCA CCT CTC TGA A-3′, R-5′-TTT CTG ATC CAC GGC TCC TGT GA-3′; *Resistin*, F-5′-AAG AAC CTT TCA TTT CCC CT-3′, R-5′-GTC CAG CAA TTT AAG CCA ATG-3′; *Runx1*, F-5′-TCT GCA GAA CTT TCC AGT CGA CTC T-3′, R-5′-TCT GGA AGG GCC CGG CCT GCG CCT-3′; *Runx2*, F-5′-CAG CAC TCC ATA TCT CTA CT-3′, R-5′-CAG CGT CAA CAC CAT CAT TC-3′; *Runx3*, F-5′-AAG ATA GAA GAC CAG ACC AAG GCC T-3′, R-5′-ACT GGC GGG GGT CGG AGA AGG GGT-3′; *Ucp1*, F-5′-CCA GGC TTC CAG TAC CAT TA-3′, R-5′-AGA AGT ACT CTT GGA CTG AG-3′; *Wwp2*, F-5′-GGA GAT AGA CAT GAG CGA CTG G-3′, R-5′-CAA CAG GCA GAC GGC AGG T-3′.

Immunofluorescences

Cells cultured on coverslips were washed once with Dulbecco's PBS (DPBS) and then fixed for 20 min in DPBS containing 4% paraformaldehyde (PFA) at room temperature. Fixed cells were permeabilized by 0.1% Triton X-100 for 5 min and then blocked by 2% bovine serum albumin for 30 min. Finally, cells were stained with first antibodies followed by FITC-conjugated or Alexa Fluor 647-conjugated secondary antibodies. Immunofluorescence images were captured using Leica SP5 (Leica LAS-AF-Lite).

Coimmunoprecipitation and endogenous protein complex isolations

Coimmunoprecipitation experiments were carried out in HEK293T cells. In briefly, cells were transfected with indicated constructs for 24 h and then lysed in a cell lysis buffer (20 mM Tris–HCl, pH 7.5, 150 mM NaCl, 1% Triton X-100, 0.5 mM EDTA, protease inhibitor cocktail [Roche], and phosphatase

inhibitor cocktail [Roche]). After centrifugation, the supernatants were pulled down by indicated antibodies and then analyzed by immunoblotting. For size-exclusion chromatography assay of endogenous protein complexes in mouse inguinal WAT, the WAT depots of 10 mice (6 weeks old)were harvested, minced, and homogenized in 20 mM Tris–HCl, pH 7.5, 150 mM NaCl, 0.5% Triton X-100, 0.5 mM EDTA, protease inhibitor cocktail, and phosphatase inhibitor cocktail. The protein complexes were isolated according to their molecular weight using a Superose 6 10/300 GL column on fast protein liquid chromatography.

Ubiquitination analysis

Indicated constructs were cotransfected into HEK293T cells along with His-ubiquitin for 24 h, and then cells were harvested in a denaturing buffer (6 M guanidine hydrochloride, 0.1 M Na_2HPO_4/NaH_2PO_4, pH 8.0, 10 mM imidazole). The lysates were then incubated with nickel–nitrilotriacetic acid resin for 3 h, followed by four time washes with the denaturing buffer and two times with a low-salt buffer (25 mM Tris–HCl, pH 6.8, 20 mM imidazole). Ubiquitinated proteins were eluted by boiling in the SDS-sample buffer in the presence of 200 mM imidazole. After centrifugation, the supernatants were analyzed by immunoblotting.

Protein tyrosine phosphorylation assays

Cells were lysed in a lysis buffer (20 mM Tris–HCl, pH 7.5, 250 mM NaCl, 1% Triton X-100, 0.1% SDS, 0.5 mM EDTA, protease inhibitor cocktail, and phosphatase inhibitor cocktail) and then followed by sonication for two times. After centrifugation, the supernatants were pulled down and analyzed by immunoblotting using a pan phosphotyrosine antibody (4G10).

ChIP

The ChIP assays were carried out as according to the manufacturer's instructions with the SimpleChIP Plus Kit (Cell Signaling). For ChIP assays in subcutaneous inguinal WAT, the adipose depots from 10 mice (6 weeks old) were harvested, minced, and fixed with 2% PFA in DPBS at 4 °C for overnight. After removing PFA solution, adipose depots were grinded in liquid nitrogen and then sonicated for 10 s to be resuspended in 1 ml of DPBS. After centrifugation, the insoluble materials containing fixed protein–DNA complexes were further extracted by chloroform to remove fatty oil and again grinded in liquid nitrogen. The last grinded insoluble materials were resuspended in an SDS lysis buffer (50 mM Tris–HCl, pH 8.1, 1% SDS, and 10 mM EDTA), and then ChIP was carried out as described in the ChIP Immunoprecipitation Assay Kit. The primers for *Ucp1* promoter DNA: −620/−830 bps (R1), F-5′-TCT GTC CTT CCA GGG CTC CTG-3′, R-5′-TTC AAA TGT CAC CTT CAG ATT T-3′; −2580/−2789 bps (R2), F-5′-TAA ATG GTG TTC TAC ATC TTA A-3′, R-5′-AAA GTT TGC CTC ATA ATG GAG A-3′; −5840/−6100 bps (R3), F-5′-AAA TCA GTG AGA AAT CCA AAG GGC TTT-3′, R-5′-GGT CAA AAA TCT TTG TTT CCA TAC AC-3′; −7770/−7902 bps (R4), F-5′-GGC CTC GTG ACT CAC AGA GGT-3′, R-5′-TGC TCT TCC AGG CAA AAC AGT-3′; −8491/−8526 bps (R5), F-5′-ACT CAG AAC AGC ACA CGT GT-3′, R-5′-AAT GAA GAC CTG TGT CTG GT-3′. For re-ChIP experiments, the protein–DNA crosslinked complexes were eluted by 10 mM of dithiothreitol in a solution of 20 mM Tris–HCl, pH 8.0, 1.0 mM EDTA from Protein G agarose beads. The primers for *Fndc5* promoter DNA: F-5′-CTA TCT GAC CCC TCT CTT TC-3′, R-5′-CCA CCC CAG CAC CAT CTG T-3′; nested primers: F-5′-ATA GCC AAC CGA AGA GAC TCC A-3′, R-5′-GCC ACA TAC CTT GTC CTG GGG G-3′.

Cell differentiation

Brown adipocyte differentiation was performed as described (42). At 70% of confluence, ADSCs isolated from BAT were grown in culture media with 20 nM of insulin (Sigma) and 1 nM of T3 (Sigma). Becoming 100% confluence, cells were induced by 1 μM of dexamethasone (Sigma), 0.5 mM of isobutyl-1-methylxanthine (Sigma), 0.125 mM of indomethacin (Sigma), 20 nM of insulin, and 1 nM of T3. About 2 days of induction, cells were maintained in culture medium with 20 nM of insulin and 1 nM of T3 for 4 to 6 days. For white adipocyte differentiation, confluent cells (ADSCs isolated from WAT, 3T3-L1, or C3H10T1/2) were induced with 1 μM of dexamethasone, 0.5 mM of isobutyl-1-methylxanthine, and 870 nM of insulin for 2 days. After induction, cells were maintained in medium containing 870 nM of insulin for 4 to 6 days (55). The differentiation of primary osteoblasts was carried out as previously described (35).

In vitro *culture of adipose tissues*

The inguinal WATs were harvested from 6-week-old male mice under aseptic conditions and cut into 0.5 mm pieces in Dulbecco's modified Eagle's medium. Agarose powder was dissolved in water at 1.5% (w/v) and autoclaved, and then agarose solution was poured into a Petri dish. After cooling, the gel was cut into 0.5 cm pieces to make agarose gel block for adipose tissue culturing. Before tissue culture, the gel blocks were presoaked in the culture medium overnight, and then the fresh tissue pieces were placed on the gel block that is half immersed in the fresh medium, 37 °C, 5% CO_2.

Statistical analysis

Two-tailed Student's t test and ANOVA were used to evaluate statistical significance and $p < 0.05$ to declare a statistically change. All values were presented as the means ± SD.

Data availability

All representative data are contained within the article.

Acknowledgments—We thanked Yalin Huang and Jin Li for confocal microscopy technical help.

Author contributions—G. X. Q., W. J. Y., H. X. Y., and H. Y. methodology; H. X. Y., H. Y., and P. Y. investigation; L. Q., Z. W., Y. Y. L., L. X. Y., and W. M. X. formal analysis; G. X. Q. and W. J. Y. writing–original draft; G. X. Q. and W. J. Y. supervision; G. X. Q. and W. J. Y. project administration.

Funding and additional information—This work was sponsored by the National Natural Science Foundation of China (grant no.: 31872829 [to G. X. Q.]).

Conflict of interest—The authors declare that they have no conflicts of interest with the contents of this article.

Abbreviations—The abbreviations used are: ADSC, adipose-derived stem cell; AR, adrenergic receptor; BAT, brown adipose tissue; cDNA, complementary DNA; ChIP, chromatin immunoprecipitation; DPBS, Dulbecco's PBS; FAK, focal adhesion kinase; FBS, fetal bovine serum; FNDC5, fibronectin type III domain–containing protein 5; HEK293T, human embryonic kidney 293T cell line; ns-Irisin, nonsecretory irisin; OCN, osteocalcin; PFA, paraformaldehyde; PGC1α, peroxisome proliferator–activated receptor γ coactivator-1α; PPARγ, peroxisome proliferator–activated receptor γ; PRDM16, PR domain–containing protein 16; PTU, propylthiouracil; qRT, quantitative RT; RHD, runt homology domain; RUNX1/2, runt-related transcriptional factors 1/2; s-Irisin, hormone-like irisin; T3, triiodothyronine; T4, tetraiodothyronine; THR, thyroid hormone receptor; TRE1/2, thyroid hormone response element 1/2; UCP1, uncoupling protein 1; WAT, white adipose tissue; WWP2, WW domain–containing protein 2.

References

1. Virtanen, K. A., Lidell, M. E., Orava, J., Heglind, M., Westergren, R., Niemi, T., Taittonen, M., Laine, J., Savisto, N. J., Enerbäck, S., and Nuutila, P. (2009) Functional brown adipose tissue in healthy adults. *N. Engl. J. Med.* **360**, 1518–1525
2. Cypess, A. M., Lehman, S., Williams, G., Tal, I., Rodman, D., Goldfine, A. B., Kuo, F. C., Palmer, E. L., Tseng, Y. H., Doria, A., Kolodny, G. M., and Kahn, C. R. (2009) Identification and importance of brown asipose tissue in adults humans. *N. Engl. J. Med.* **360**, 1509–1517
3. Enerback, S. (2010) Human brown adipose tissue. *Cell Metab.* **11**, 248–252
4. Wu, J., Boström, P., Sparks, L. M., Ye, L., Choi, J. H., Giang, A. H., Khandekar, M., Virtanen, K. A., Nuutila, P., Schaart, G., Huang, K., Tu, H., van Marken Lichtenbelt, W. D., Hoeks, J., Enerbäck, S., *et al.* (2012) Beige adipocytes are a distinct type of thermogenic fat cell in mouse and human. *Cell* **150**, 66–376
5. Himms-Hagen, J., Melnyk, A., Zingaretti, M. C., Ceresi, E., Barbatelli, G., and Cinti, S. (2000) Multilocular fat cells in WAT of CL-316243-treated rats derive directly from white adipocytes. *Am. J. Physiol. Cell Physiol.* **279**, C670–C681
6. Fisher, F. M., Kleiner, S., Douris, N., Fox, E. C., Mepani, R. J., Verdeguer, F., Wu, J., Kharitonenkov, A., Flier, J. S., Maratos-Flier, E., and Spiegelman, B. M. (2012) Fgf21 regulates PGC-1α and browning of white adipose tissues in adaptive thermogenesis. *Genes Dev.* **26**, 271–281
7. Li, Q., Hua, Y., Yang, Y. L., He, X. Y., Zhu, W., Wang, J. Y., and Gan, X. Q. (2018) T cell factor 7 (TCF7)/TCF1 feedback controls osteocalcin signaling in brown adipocytes independent of the Wnt/β-Catenin pathway. *Mol. Cell. Biol.* **38**, e00562-17
8. Boström, P., Wu, J., Jedrychowski, M. P., Korde, A., Ye, L., Lo, J. C., Rasbach, K. A., Boström, E. A., Choi, J. H., Long, J. Z., Kajimura, S., Zingaretti, M. C., Vind, B. F., Tu, H., Cinti, S., *et al.* (2012) A PGC1-α-dependent myokine that drives brown-fat-like development of white fat and thermogenesis. *Nature* **481**, 463–469
9. Xiong, Y., Wu, Z., Zhang, B., Wang, C., Mao, F., Liu, X., Hu, K., Sun, X. B., Jin, W., and Kuang, S. (2019) Fndc5 loss-of- function attenuates exercise-induced browning of white adipose tissue in mice. *FASEB J.* **33**, 5876–5886
10. Luo, Y. Y., Qiao, X. Y., Ma, Y. X., Deng, H. X., Xu, C. C., and Xu, L. Z. (2020) Disordered metabolism in mice lacking irisin. *Sci. Rep.* **10**, 17368
11. Ellefsen, S., Vikmoen, O., Slettalokken, G., Whist, J. E., Nygaard, H., Hollan, I., Rauk, I., Vegge, G., Strand, T. A., Raastad, T., and Ronnestad, B. R. (2014) Irisin and FNDC5: Effects of 12-week strength training, and relations to muscle phenotype and body mass composition in untrained women. *Eur. J. Appl. Physiol.* **114**, 1875–1888
12. Bonfante, I. L. P., Chacon-Mikahil, M. P. T., Brunelli, D. T., Gaspari, A. F., Duft, R. G., Lopes, W. A., Bonganha, V., Libardi, C. A., and Cavaglieri, C. R. (2017) Combined training, FNDC/irisin levels and metabolic markers in obese man: A randomized controlled trial. *Eur. J. Sport Sci.* **17**, 629–637
13. Staiger, H., Bohm, A., Scheler, M., Berti, L., Machann, J., Schick, F., Machicao, F., Fritsche, A., Stefan, N., Weigert, C., Krook, A., Haring, H. U., and de Angelis, M. H. (2013) Common genetic variation in the human *FNDC5* locus, encoding the novel muscle-derived 'browning' factor irisin, determines insulin sensitivity. *PLoS One* **8**, e61903
14. Al-Daghri, N. M., Mohammed, A. K., AL-Attas, O. S., Amer, O. E., Clerici, M., Alenad, A., and Alokail, M. S. (2016) SNPs in FNDC (irisin) are associated with obesity and modulation of glucose and lipid metabolism in Saudi subjects. *Lipids Health Dis.* **15**, 54
15. Abdu Allah, A. M., Hammoudah, S. A., Abd EI Gayed, E. M., El-Attar, L. M., and Shehab-Eldin, W. A. (2018) Obesity and its association with irisin level among individuals with FNDC5/irisin gene variants RS16835198 and RS726344. *Protein Pept. Lett.* **25**, 560–569
16. Colaianni, G., Cuscito, C., Mongelli, T., Pignataro, P., Buccoliero, C., Liu, P., Lu, P., Sartini, L., Di Comite, M., Mori, G., Di Benedetto, A., Brunetti, G., Yuen, T., Sun, L., Reseland, J. E., *et al.* (2015) The myokine irisin increases cortical bone mass. *Proc. Natl. Acad. Sci. U. S. A.* **112**, 12157–12162
17. Colaianni, G., Mongelli, T., Cuscito, C., Pignataro, P., Lippo, L., Spiro, G., Notarnicola, A., Severi, I., Passeri, G., Mori, G., Brunetti, G., Moretti, B., Tarantino, U., Colucci, S. C., Reseland, J. E., *et al.* (2017) Irisin prevents and restores bone loss and muscle atrophy in hind-limb suspended mice. *Sci. Rep.* **7**, 2811
18. Anastasilakis, A. D., Polyzos, S. A., Makras, P., Gkiomisi, A., Bistinas, I., Katsarou, A., Filippaios, A., and Mantzoros, C. S. (2014) Circulating irisin is associated with osteoporotic fractures in postmenopausal women with low bone mass but is not affected by either teriparatide or denosumab treatment for 3 months. *Osteoporos. Int.* **25**, 1633–1642
19. Palermo, A., Strollo, R., Maddaloni, E., Tuccinardi, D., D'Onofrio, L., Briganti, S. I., Defeudis, G., De Pascalis, M., Lazzaro, M. C., Colleluori, G., Manfrini, S., Pozzilli, P., and Napoli, N. (2015) Irisin is associated with osteoporotic fractures indenpendently of bone mineral density, body composition or daily physical activity. *Clin. Endocrinol. (Oxf.)* **82**, 615–619
20. Colaianni, G., Faienza, M. F., Sanesi, L., Brunetti, G., Pignataro, P., Lippo, L., Bortolotti, S., Storlino, G., Piacente, L., D'Amato, G., Colucci, S., and Grano, M. (2019) Irisin serum levels are positively correlated with bone mineral status in a population of healthy children. *Pediatr. Res.* **85**, 484–488
21. Faienza, M. F., Brunetti, G., Sanesi, L., Cloaianni, G., Celi, M., Piacente, L., D'Amato, G., Schipani, E., Colucci, S., and Grano, M. (2018) High irisin levels are associated with better glycemic control and bone health in children with type 1 diabetes. *Diabetes Res. Clin. Pract.* **141**, 10–17
22. Grygiel-Gorniak, B., and Puszczewicz, M. (2017) A review on irisin, a new protagonist that mediated muscle-adipose-bone-neuron connectivity. *Eur. Rev. Med. Pharmacol. Sci.* **21**, 4687–4693
23. Martinez Munoz, I. Y., Camarillo Romero, E. D. S., and Garduno Garcia, J. J. (2018) Irisin a novel metabolic biomarker: Present knowledge and future directions. *Int. J. Endocrinol.* **2018**, 7816806

24. Zhang, Y., Li, R., Meng, Y., Li, S. W., Donelan, W., Zhao, Y., Qi, L., Zhang, M. X., Wang, X. L., Cui, T. X., Yang, L. J., and Tang, D. Q. (2014) Irisin stimulates browning of white adipocytes through mitogen-activated protein kinase p38 MAP kinase and ERK MAP kinase signaling. *Diabetes* **63**, 514–525
25. Li, D. J., Li, Y. H., Yuan, H. B., Qu, L. F., and Wang, P. (2017) The novel exercise-induced hormone irisin protects against neuronal injury via activation of the Akt and ERK1/2 signaling pathways and contributes to the neuroprotection of physical exercise in cerebral ischemia. *Metabolism* **68**, 31–42
26. Rabiee, F., Lachinani, L., Ghaedi, S., Nasr-Esfahani, M. H., Megraw, T. L., and Ghaedi, K. (2020) New insights into the cellular activities of Fndc5/irisin and its signaling pathways. *Cell Biosci.* **10**, 51
27. Liu, T. Y., Xiong, X. Q., Ren, X. S., Zhao, M. X., Shi, C. X., Wang, J. J., Zhou, Y. B., Zhang, F., Han, Y., Gao, X. Y., Chen, Q., Li, Y. H., Kang, Y. M., and Zhu, G. Q. (2016) FNDC5 alleviates hepatosteatosis by restoring AMPK/mTOR-mediated autophagy, fatty acid oxidation, and lipogenesis in mice. *Diabetes* **65**, 3262–3275
28. Oguri, Y., Shinoda, K., Kim, H., Alba, D. L., Bolus, W. R., Wang, Q., Brown, Z., Pradhan, R. N., Tajima, K., Yoneshiro, T., Ikeda, K., Chen, Y., Cheang, R. T., Tsujino, K., Kim, C. R., *et al.* (2020) CD81 controls beige fat progenitor cell growth and energy balance via FAK signaling. *Cell* **182**, 563–577
29. Ponrartana, S., Aggabao, P. C., Hu, H. H., Aldrovandi, G. M., Wren, T. A. L., and Gilsanz, V. (2012) Brown adipose tissue and its relationship to bone structure in pediatric patients. *J. Clin. Endocrinol. Metab.* **97**, 2693–2698
30. Lee, P., Brychta, R. J., Collins, M. T., Linderman, J., Smith, S., Herscovitch, P., Millo, C., Chen, K. Y., and Celi, F. S. (2013) Cold-activated brown adipose tissue is an independent predictor of higher bone mineral density in women. *Osteoporos. Int.* **24**, 1513–1518
31. Bredella, M. A., Gill, C. M., Rosen, C. J., Klibanski, A., and Torriani, M. (2014) Positive effects of brown adipose tissue on femoral bone structure. *Bone* **58**, 55–58
32. Colaianni, G., Errede, M., Sanesi, L., Notarnicola, A., Celi, M., Zerlotin, R., Storlino, G., Pignataro, P., Oranger, A., Pesce, V., Tarantino, U., Moretti, B., and Grano, M. (2021) Irisin correlates positively with BMD in a cohort of older adult patients and downregulates the senescent marker p21 in osteoblasts. *J. Bone Miner. Res.* **36**, 305–314
33. Puigserver, P., Wu, Z., Park, C. W., Graves, R., Wright, M., and Spiegelman, B. M. (1998) A cold- inducible coactivator of nuclear receptors linked to adaptive thermogenesis. *Cell* **92**, 829–839
34. Himms-Hagen, J., Cui, J., Danforth, E., Jr., Taatjes, D. J., Lang, S. S., Waters, B. L., and Claus, T. H. (1994) Effect of CL-316243, a thermogenic beta3-agonist, on energy balance and brown and white adipose tissues in rats. *Am. J. Physiol.* **266**, R1371–R1382
35. Zhu, W., He, X. Y., Hua, Y., Li, Q., Wang, J. Y., and Gan, X. Q. (2017) E3 ubiquitin ligase WWP2 facilitates RUNX2 transactivation through a mono-ubiquitination manner during osteogenic differentiation. *J. Biol. Chem.* **292**, 11178–11188
36. Cohen, P., Levy, J. D., Zhang, Y. Y., Frontini, A., Kolodin, D. P., Svensson, K. J., Lo, J. C., Zeng, X., Ye, L., Khandekar, M. J., Wu, J., Gunawardana, S. C., Banks, A. S., Camporez, J. P., Jurczak, M. J., *et al.* (2014) Ablation of PRDM16 and beige adipose causes metabolic dysfunction and a subcutaneous to visceral fat switch. *Cell* **156**, 304–316
37. Huh, J. Y., Panagiotou, G., Mougios, V., Brinkoetter, M., Vamvini, M. T., Schneider, B. E., and Mantzoros, C. S. (2012) FNDC5 and irisin in humans: I. Predictors of circulating concentrations in serum and plasma and II. mRNA expression and circulating concentrations in response to weight loss and exercise. *Metabolism* **61**, 1725–1738
38. Bousmpoula, A., Benidis, E., Demeridou, S., Kapeta-Kourkouli, R., Chasiakou, A., Chasiakou, S., Kouskouni, E., and Baka, S. (2019) Serum and follicular fluid irisin levels in women with polycystic ovaries undergoing ovarian stimulation: Correlation with insulin resistance and lipoprotein lipid profiles. *Gynecol. Endocrinol.* **35**, 803–806
39. Jia, J., Yu, F., Wei, W. P., Yang, P., Zhang, R., Sheng, Y., and Shi, Y. Q. (2019) Relationship between circulating irisin levels and overweight/obesity: A meta-analysis. *World J. Clin. Cases* **7**, 1444–1455
40. Karampatsou, S. I., Genitsaridi, S. M., Michos, A., Kourkouni, E., Kourlaba, G., Kassari, P., Manios, Y., and Charmandari, E. (2021) The effect of a life-style intervention program of diet and exercise on irisin and FGF-21 concentrations in children and adolescents with overweight and obesity. *Nutrients* **13**, 1274
41. Moreno-Navarrete, J. M., Ortega, F., Serrano, M., Guerra, E., Pardo, G., Tinahones, F., Ricart, W., and Fernández-Real, J. M. (2013) Irisin is expressed and produced by human muscle and adipose tissue in association with obesity and insulin resistance. *J. Clin. Endocrinol. Metab.* **98**, E769–E778
42. Seale, P., Bjork, B., Yang, W., Kajimura, S., Chin, S., Kuang, S., Scime, A., Devarakonda, S., Conroe, H. M., Erdjument-Bromage, H., Tempst, P., Rudnicki, M. A., Beier, D. R., and Spiegelman, B. M. (2008) PRDM16 controls a brown fat/skeletal muscle switch. *Nature* **454**, 961–967
43. Lee, P., Linderman, J., Smith, S., Brychta, R. J., Wang, J., Idelson, C., Perron, R. M., Werner, C. D., Phan, G. Q., Kammula, U. S., Kebebew, E., Pacak, K., Chen, K. Y., and Celi, F. S. (2014) Irisin and FGF21 are cold-induced endocrine activators of brown fat function in humans. *Cell Metab.* **19**, 302–309
44. Backstrom, S., Wolf-Watz, M., Grundstrom, C., Hard, T., Grundstrom, T., and Sauer, U. H. (2002) The RUNX1 runt domain at 1.25A resolution: A structural switch and specifically bound chloride lons modulate DNA binding. *J. Mol. Biol.* **322**, 259–272
45. Greaves, M. (2018) A causal mechanism for childhood acute lymphoblastic leukaemia. *Nat. Rev. Cancer* **18**, 471–484
46. Komori, T. (2005) Regulation of skeletal development by the runx family of transcription factors. *J. Biol. Biochem.* **95**, 445–453
47. Zou, W. G., Chen, X., Shim, J., Huang, Z. W., Brady, N., Hu, D., Drapp, R., Sigrist, K., Glimcher, L. H., and Jones, D. (2011) The E3 ubiquitin ligase Wwp2 regulates craniofacial development through mono-ubiquitination of Goosecoid. *Nat. Cell Biol.* **13**, 59–65
48. Nakamura, Y., Yamamoto, K., He, X. J., Otsuki, B., Kim, Y., Murao, H., Soeda, T., Tsumaki, N., Deng, J. M., Zhang, Z. P., Behringer, R. R., Crombrugghe, B. D., Postlethwait, J. H., Warman, M. L., Nakamura, T., *et al.* (2011) Wwp2 is essential for palatogenesis mediated by the interaction between Sox9 and mediator subunit 25. *Nat. Commun.* **2**, 251
49. Ott, C. E., Leschik, G., Trotier, F., Brueton, L., Brunner, H. G., Brussel, W., Guillen-Navarro, E., Haase, C., Kohlhase, J., Kotzot, D., Lane, A., Lee-Kirsch, M. A., Morlot, S., Simon, M. E., Steichen-Gersdorf, E., *et al.* (2010) Deletions of the *RUNX2* gene are present in about 10% of individuals with cleidocranial dysplasia. *Hum. Mutat.* **31**, E1587–E1593
50. Bjork, B. C., Turbe-Doan, A., Prysak, M., Hurron, B. J., and Beier, D. R. (2010) *Prdm16* is required for normal palatogenesis in mice. *Hum. Mol. Genet.* **19**, 774–789
51. Vadala, G., Di Giacomo, G. D., Ambrosio, L., Cannata, F., Cicione, C., Papalia, R., and Denaro, V. (2020) Irisin recovers osteoarthritic chondrocytes *in vitro*. *Cell* **9**, 1478
52. Wang, F. S., Kuo, C. W., Ko, J. Y., Chen, Y. S., Wang, S. Y., Ke, H. J., Kuo, P. C., Lee, C. H., Wu, J. C., Lu, W. B., Tai, M. H., Jahr, H., and Lian, W. S. (2020) Dysfunction and osteoarthritis development through regulating mitochondrial integrity and autophagy. *Antioxidants (Basel)* **9**, 810
53. Karsenty, G. (2017) Update on the biology of osteocalcin. *Endocr. Pract.* **23**, 1270–1274
54. Tseng, Y. H., Kriauciunas, K. M., Kokkotou, E., and Kahn, C. R. (2004) Differential roles of insulin receptor substrates in brown adipocyte differentiation. *Mol. Cell. Biol.* **24**, 1918–1929
55. Vernochet, C., Peres, S. B., Davis, K. E., McDonald, M. E., Qiang, L., Wang, H., Scherer, P. E., and Farmer, S. R. (2009) C/EBPα and the corepressors CtBP1 and CtBP2 regulate repression of select visceral white adipose genes during induction of the brown phenotype in white adipocytes by peroxisome proliferator-activated receptor γ agonists. *Mol. Cell. Biol.* **29**, 4714–4728